LISA MARX

POSITRONIUM FORMATION IN POROUS MATERIALS FOR ANTIHYDROGEN PRODUCTION

Test of detectors and targets

Master Thesis

Graz University of Technology
Institute of Materials Physics

Supervisor: Univ.-Prof.Dr. Roland Würschum (TU Graz)
In cooperation with the AEgIS positron group/ CERN
Co-Supervisor: Dr. Sebastiano Mariazzi (CERN)

Graz, March 2016

This document is set in Palatino, compiled with pdfLaTeX2e and `Biber`.

The LaTeX template from Karl Voit is based on KOMA script and can be found online: https://github.com/novoid/LaTeX-KOMA-template

Statutory Declaration

I declare that I have authored this thesis independently, that I have not used other than the declared sources/resources, and that I have explicitly marked all material which has been quoted either literally or by content from the used sources.

Graz, _____ _____

Date Signature

Eidesstattliche Erklärung[1]

Ich erkläre an Eides statt, dass ich die vorliegende Arbeit selbstständig verfasst, andere als die angegebenen Quellen/Hilfsmittel nicht benutzt, und die den benutzten Quellen wörtlich und inhaltlich entnommenen Stellen als solche kenntlich gemacht habe.

Graz, am _____ _____

Datum Unterschrift

[1] Beschluss der Curricula-Kommission für Bachelor-, Master- und Diplomstudien vom 10.11.2008; Genehmigung des Senates am 1.12.2008

Abstract

To be the first to measure the effect of the earths gravitational force on antihydrogen atoms, the AEgIS collaboration (Antimatter Experiment: Gravity, Interferometry, Spectroscopy) at CERN is working on the realization of a cold antihydrogen beam, by mixing a cold antiproton plasma with Rydberg excited positronium and transporting the formed antihydrogen atoms via Stark-acceleration towards a moiré deflectometer to detect the displacement of the antihydrogen beam caused by gravity. This master thesis focuses on the production of positronium for antihydrogen production.

To test different positron/positronium converters used for Ps production in the AEgIS positron system, one part of the measurements was conducted at the VEPAS (Variable Energy Positron Annihilations Spectroscopy) slow positron beam in Como. Two different silicon-based samples with different nanochannel orientation and doping were measured via positronium spectroscopy. A Ps fraction of 50% was obtained for the p-type(111) sample and fraction of 5% for the n-type(100) sample. The high positronium yield marks the p-type(111) sample as a well suitable positron/positronium converter.
In addition initial tests of two diesel particulate filter samples were conducted. These samples were provided by the AVL (Anstalt für Verbrennungskraftmaschinen List) in Graz, consisting of a Nickel substrate with and without a deposited carbon layer and were examined through Doppler Broadening spectroscopy and positronium spectroscopy.

Secondly, the e^+/Ps converters were tested in the AEgIS positron system via SSPALS (Single shot positron annihilation lifetime spectroscopy). Three different silicon based positronium targets with nanochannels were compared, namely a p-type (111) and n-type (100) sample, identical to the samples measured by

Doppler broadening, and a p-type (100) sample. No positronium emission could be measured for the n-type(100) sample, for the p-type(100) sample a positronium lifetime of 111 ± 1 ns was measured and for the p-type(111) target the lifetime amounts to 142 ± 1 ns. These results are consistent with the measurements made at the VEPAS laboratory in Como and highlight the p-type(111) sample as the most suitable target for positronium production.

To supply positrons for positronium production, the systematic optimization of the AEgIS positron apparatus was necessary. Therefore, a buncher for positron compression was included and the most suitable detector for positronium detection was investigated. The positron beam diameter could be compressed to one third of the initial value and a well suitable detector ($PbWO_4$ scintillator coupled to a R11265-100 PMT) for positronium detection was determined.

Abstract

Um den Effekt des Erdgravitationsfeldes auf Antiwasserstoffatome zu messen, arbeitet die AEgIS Kollaboration (Antimatter Experiment: Gravity, Interferometry, Spectroscopy) am CERN an der Realisierung eines kalten Antiwasserstoffstrahls durch Mixen eines kalten Antiproton-Plasmas mit Rydberg-angeregtem Positronium und Transport der erzeugten Antiwasserstoffatome über Stark-Beschleunigung auf ein Moiré-Deflektometer. Ziel ist es, die Verschiebung des Antiwasserstoffstrahls durch die Gravitation zu detektieren. Der Schwerpunkt dieser Masterarbeit ist die Herstellung von Positronium für die Produktion von Antiwasserstoff.

Um verschiedene Positron/Positroniumkonverter für die Positroniumproduktion am AEgIS Positronensystem zu testen, wurde ein Teil der Messungen am VEPAS (Variable Energy Positron Annihilations Spectroscopy) slow-positron-Strahl in Como/Italien durchgeführt. Zwei unterschiedliche Silizium-basierte Proben mit unterschiedlicher Channel-Orientierung und Dotierung wurden mittels Positroniumspektroskopie untersucht. Ein Positronium-Anteil von 50% wurde für die p-Typ(111) Probe gemessen und ein Anteil von 5% für die n-Typ(100) Probe. Die hohe Positroniumausbeute macht das p-Typ(111) Target zu einem gut geeigneten Positronen/Positronium Konverter.
Des weiteren wurden erste Tests zweier Dieselfilterproben durchgeführt. Die Proben wurden von der AVL (Anstalt für Verbrennungskraftmaschinen List) in Graz zur Verfügung gestellt und bestanden aus einem Nickel-Substrat mit und ohne aufgebrachter Rußschicht. Die Messungen wurden mittels Dopplerverbreiterungsspektroskopie und Positroniumspektroskopie durchgeführt.
Ferner wurden die e^+/Ps Konverter am AEgIS-Positronensystem via SSPALS (Single shot positron annihilation lifetime spectroscopy) getestet. Drei unterschiedliche Silizium-basierte Proben mit Nanochannels wurden verglichen, eine

p-Typ(111) Probe und eine n-Typ(100) Probe, identisch zu den mittels Doppler-Verbreiterung vermessenen Proben. Zusätzlich wurde ein p-Typ(100) Target getestet. Für die n-Typ(100) Probe konnte keine Positronium-Emission gemessen werden, für die p-Typ(100) Probe wurde eine Positronium-Lebensdauer von 111 ± 1 ns ermittelt und für das p-Typ(111) Target ergab die Lebensdauer 142 ± 1 ns. Diese Ergebnisse stimmen mit den am VEPAS-Labor in Como durchgeführten Messungen überein und heben die p-Typ(111) Probe als bestgeeignetes Target hervor.

Um Positronen zur Positroniumproduktion zur Verfügung zu stellen war eine Optimierung des AEgIS Positronensystems notwendig. Ein Buncher zur Positronen-Kompression wurde installiert. Des weiteren wurde der bestgeeignete Detektor zur Detektion von Positronium ermittelt. Der Positronenbeam-Durchmesser konnte zu einem Drittel des Ausgangswertes komprimiert werden und ein gut geeigneter Detektor ($PbWO_4$ Szintillator gekoppelt mit einem R11265-100 PMT) zur Detektion von Positronium wurde ermittelt.

Contents

1 Fundamentals **3**

1.1 Antimatter . . . 3

1.1.1 Positrons . . . 4

1.2 Positron Sources and Positron Moderation . . . 7

1.2.1 Sources . . . 7

1.2.2 Moderators . . . 7

1.3 Trapping and Cooling of Positrons . . . 9

1.4 Positronium . . . 10

1.5 Detectors . . . 12

1.5.1 Plastic or Crystal Scintillators . . . 13

1.5.2 Cherenkov Radiators . . . 14

1.5.3 Multi-Channel Plate and Phosphor Screen . . . 15

1.5.4 Semiconductor Detector . . . 16

1.6 Measuring methods of e^+e^--annihilation . . . 16

1.6.1 Positron annihilation lifetime spectroscopy . . . 16

1.6.2 PALS with pulsed e^+ beam . . . 17

1.6.3 Doppler Broadening Spectroscopy . . . 18

1.6.4 Ortho-Positronium Spectroscopy . . . 20

1.7 Laser excitation . . . 22

2 Experimental Setup **23**

2.1 CERN and the AEgIS-Experiment . . . 23

2.1.1 Production of antihydrogen . . . 24

2.1.2 Overview of the AEgIS Main Magnets Region . . . 25

2.2 The AEgIS-Positron system . . . 26

2.2.1 System Overview . . . 27

2.2.2 ^{22}Na Source and Solid Neon Moderator . . . 29
2.2.3 Positron Trap . . . 31
2.2.4 Accumulator . . . 33
2.2.5 Buncher . . . 34
2.2.6 Detection of Positrons/Positronium and System Calibrations 35
2.3 The AEgIS Laser System . . . 40
2.3.1 Detection of excited Positronium Atoms . . . 41
2.4 VEPAS Slow Positron Beam Experiment in Como . . . 43
2.4.1 ^{22}Na-Source, Tungsten-Moderator and e^+-Transport . . . 43
2.4.2 Detectors . . . 44
2.4.3 Data Analysis . . . 45
2.5 Positronium Targets . . . 47
2.5.1 Silicon Targets . . . 47
2.5.2 Diesel Particulate Filter Samples (AVL) . . . 49

3 Results 51
3.1 Comparison of different detectors for SSPALS . . . 51
3.2 Implementation of a buncher in the AEgIS Positron System . . . 56
3.3 Comparison of different Targets for Positronium Production . . . 63
3.3.1 SEM-Measurements of the Positronium Targets . . . 63
3.3.2 Measurements at the VEPAS Laboratory/Como . . . 66
3.3.3 Measurements at the AEgIS Experiment (CERN) . . . 73

4 Evaluation and Outlook 76
4.1 Future Work . . . 78

5 Abreviations 80

6 Acknowledgments 82

Bibliography 83

Introduction and Motivation

At CERN (French: Conseil Européen pour la Recherche Nucléaire), physicists and engineers operate the largest particle physics laboratory in the world.

Antimatter is the subject of science fiction, but antimatter is also the subject of reality. When antimatter meets matter, they immediately dissolve into pure energy. [1] According to theory, in the big bang equal amounts of matter and antimatter should have been created. When matter and antimatter come into contact they annihilate, leaving nothing but a flash of energy behind. So in principle, none of us and nothing around us should exist. But we do and as far as we can tell right now, it is only because, there was one extra matter particle for every billion matter-antimatter pairs. To explain this asymmetry, different experiments all around the world were founded and are working on shedding light on the matter-antimatter imbalance.
The principle goal of the AEgIS (Antihydrogen Experiment: Gravity, Interferometry, Spectroscopy) experiment at the European laboratory for particle physics (CERN) is the production of an antihydrogen beam for investigating matter-antimatter gravitational interaction. [2]

Even though the principle of universality of free fall (or Weak Equivalence principle)[3] has been tested with very high precision for matter, the behaviour of antiparticles in the earth's gravitational field has never directly been measured. Therefore, the goal is to produce low energy (E $<$ meV) antihydrogen atoms for high-resolution spectroscopic comparisons with hydrogen as a test of baryogenesis asymmetries [1] and charge-parity-time asymmetry [2]. These antihydrogen atoms

[1] The hypothetical processes that implicates an imbalance between baryons and antibaryons produced in the very early universe. The baryonic matter that exists today is what is left after the baryonic matter-antimatter annihilations at the beginning of the universe.
[2] A violation of the conservation of charge, parity and time. [4]

will be produced using the Antiproton Decelerator (AD) at CERN providing antiprotons and a ^{22}Na radioactive source to procure positrons which are then used for positronium production.

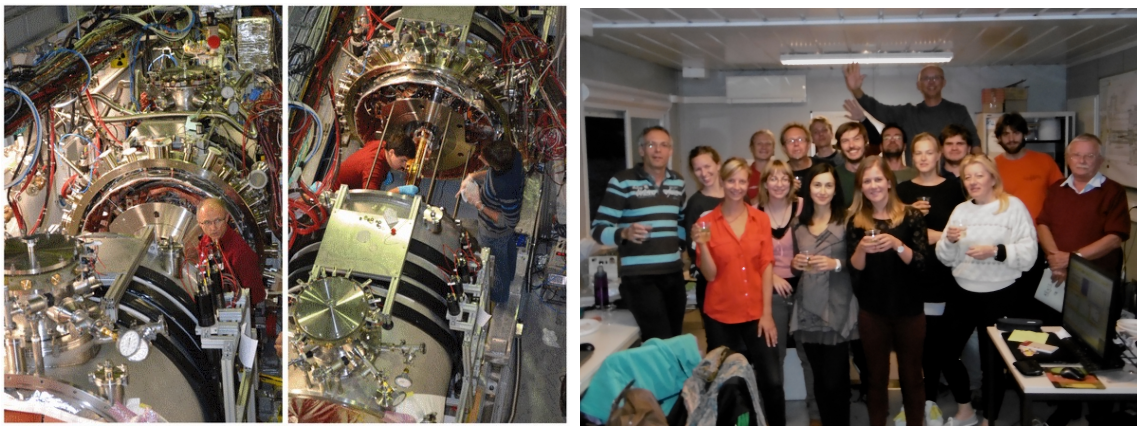

Figure 0.1: The AEgIS experiment and part of the AEgIS collaboration

This thesis focuses on the AEgIS positron system and the testing of different targets for the formation of positronium. Single shot positron annihilation lifetime spectroscopy (SSPALS) was used to study different positron/positronium converters with a high positronium yield. To create a high number of positronium atoms it was necessary to maximize the number of positrons that arrive at the target and to improve the positron beam properties by optimizing the system. Different assisting tasks were carried out during the work at the AEgIS system, like handling the cryogenic maintenance for the cooling of the magnets with Nitrogen and liquid Helium and the operation of a 10 ton overhead crane in the AD hall.

In cooperation between CERN and the AVL (Anstalt für Verbrennungskraftmaschinen List), diesel particulate filter samples with a carbon layer were characterized. Measurements were performed at one of the VEPAS groups, part of the AEgIS-Collaboration in Como/Italy, using Doppler Broadening Spectroscopy and positronium spectroscopy for the investigations of the different positronium targets and diesel particulate filter samples.

1 Fundamentals

1.1 Antimatter

In 1928 Paul Dirac predicted the positron by combining quantum theory and special relativity to describe the behaviour of an electron moving at relativistic speeds. He found that for every particle there exists a corresponding antiparticle, exactly matching the particle but with opposite charge. This equation won him the Nobel prize later on but also opened the door to a completely new chapter in physics: The subject of Antimatter studies.
When matter and antimatter come into contact with each other they annihilate immediately and dissolve into a flash of energy, mostly gamma rays, see figure 1.1. Proton/antiproton annihilation also produces particles, mesons (mainly pions).

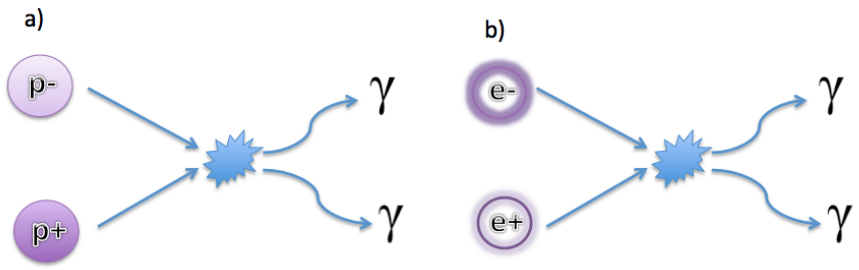

Figure 1.1: Antimatter annihilation of an electron/positron pair into two gamma-rays.

According to the current status of particle physics, particles and their antiparticles should have the exact same properties, only with opposite charge. This is called matter-antimatter symmetry.
When matter is produced according to Einstein's equation $E = mc^2$ through high energy collisions, like it happens for instance in the Large Hadron Collider at CERN, always a particle and it's corresponding antiparticle is created. But all of

the above mentioned facts lead to the question of the whereabouts of antimatter in our universe. If in the Big Bang the same amounts of matter and antimatter were created, what happened to all the antimatter since then? There are several possible answers to this question which are currently investigated. For instance, regions of the universe where antimatter dominates are searched for at the Alpha Magnetic Spectrometer (CERN) at the International Space Station and the presence of an electric dipole moment in fundamental particles is studied at the Advanced Cold Molecule Electron collaboration at Harvard. Another competing hypothesis is the difference in the effect of gravitation on matter and antimatter which is investigated at the AEgIS experiment at CERN. For historical reasons, the matter-antimatter asymmetry in the Universe is called baryon asymmetry, the production of the matter excess is called baryogenesis, see [5].

In cosmic rays, positrons and antiprotons have been observed. The biggest antimatter atom artificially produced so far is the antihelium atom, but more complex antimatter was never observed until now.
Antimatter is hard to produce and even harder to keep since it has a very limited lifetime and has to be kept in magnetic and electric traps to prevent it from annihilating with the matter around it.

1.1.1 Positrons

The positron (positive electron) representing the antiparticle of the electron, is a subatomic particle with positive charge and within experimental limits, with the same mass and magnitude of charge as the electron. The positron was the first of the antiparticles to be discovered by Carl David Anderson in cloud-chamber studies of the composition of cosmic rays in 1932. The discovery of the positron explained a theoretical aspect of electrons predicted by the Dirac wave equation in 1928.

Even though positrons are stable in vacuum, they quickly react with the electrons of ordinary matter by annihilation and production of gamma radiation.

The most common annihilation reaction is:

$$e^+ + e^- \rightarrow 2\gamma \tag{1.1}$$

If both, the annihilating electron and positron involved, are at rest, all resulting gamma rays will be emitted with an energy of 511 keV, which corresponds to the mass of the positron or electron at rest. [6]

Positron interactions in matter

A very important feature of positrons is that they are distinguishable from electrons. It is not possible to follow the diffusion history of a particular electron implanted in a target, since it disappears in the sea of identical electrons in the solid. When following positrons on the other hand, each positron annihilation can be detected. It is possible to measure the influence of different material properties, such as impurities and defects and their distributions and spatial changes in composition like layered structures.
Due to their positive charge, positrons are able to take part in many processes that are not possible for electrons: They can be trapped in lattice defects with negative charge, in open-volume defects and impurities. Also, the positron work function provides a repulsive surface-dipole contribution to the electron work function and is therefore negative for many materials. For this reason, the positrons are emitted from the surfaces of these materials and end up in the vacuum, or are trapped in large open volume defects.
Positrons are also able to bind an electron to form an exotic atom called Positronium. This hydrogen like atom can not exist in metals, due to the large number of electrons but it can exist inside of insulators and can be emitted from the surface of any kind of material.

Due to the antimatter nature of the positron, different spectroscopy methods have been developed which can not be achieved by using electrons. This methods

use the reemission of positrons from surfaces, the formation of positronium and additionally the annihilation of positrons with electrons in different materials. For the last point, the energy and angular distribution of the produced gamma rays can be used to obtain information about the environment of the annihilated positron. Also the annihilation rate indicates the structure of the probed material, through investigating whether the positron can diffuse freely or is caught in a defect or impurity. [7]
In graph 1.2 a schematic summary of the different interactions of positrons with matter can be seen.

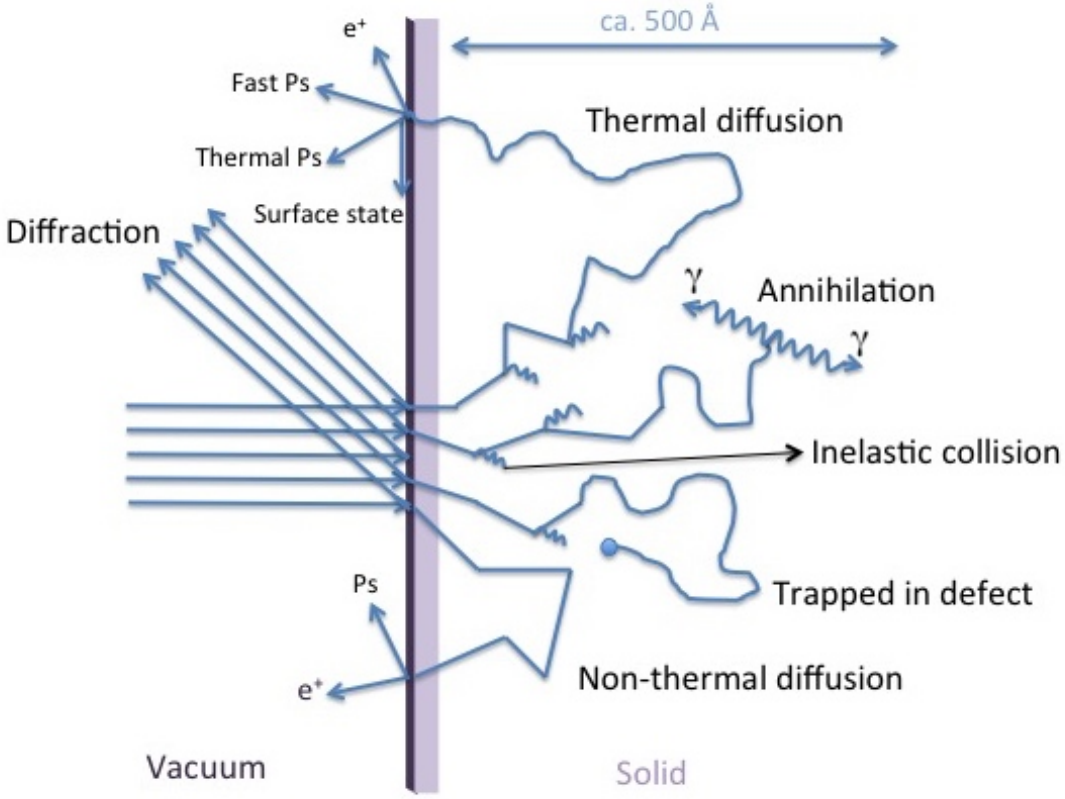

Figure 1.2: Possible positron interactions in matter

Relevant for this thesis are the annihilations from trapped states, where in large defects there is a possibility of Positronium formation, which can either annihilate inside the defect or in the case of open porosity it can propagate to the surface and reach the vacuum. On the way to the surface the Ps-atoms lose energy

through collisions with the pore walls. Also relevant are the diffusion processes, where both thermalized and non-thermalized positrons can reach the surface from which they are either emitted as positrons or, by binding an electron, as Ps. [8]

1.2 Positron Sources and Positron Moderation

1.2.1 Sources

In general there are two different methods for positron production: Pair production (for more information see [7]) and radioactive decay. The method used during the work for this thesis is the production through **radioactive decay**: Positrons are emitted in the positive beta decay of proton-rich/neutron-deficient radioactive nuclei. Generating positrons through radioactive decay is more cost efficient and more easily conducted than through the process of pair production. For most long term experiments a ^{22}Na source is used, as is done in the AEgIS and Como positron experiments. ^{22}Na offers an acceptable compromise between cost per Bq and half-life (2.6 years). ^{58}Co is used for experiments which need high beam intensity over short periods of time. It has a half-life of 71 days and offers a much higher activity for the same price as ^{22}Na does. [9] The decays of certain short-lived particles, like the positive muon are also positron sources. Positrons produced from man-made radioactive sources are used in medical diagnosis for a technique known as positron emission tomography (PET). [7]

1.2.2 Moderators

For experiments with slow positron beams, it is necessary to convert the fast e^+ provided by the source at various energies into mono-energetic slow positrons. This is executed through the use of moderators and discussed in this chapter.

The work function of positrons in different materials holds valuable information about the material itself and is due to its dependency on temperature and intrinsic stress an interesting property to study. In order to extract a positron from the surface of a material, an ionisation energy is necessary, where the minimal required energy is given by the work function. Suitable materials for positron moderation are typically (with the exception of rare gas solid moderators) characterized by their negative positron work function Φ^+ which is given in many solids.[13]

Positron Moderation

Typically positrons with a kinetic energy of a few eV are required for optimal transfer of e^+ to the trap, see section 1.3. This is most commonly achieved by using e^+ moderators placed directly after the positron source.

The most commonly used moderator is made out of a thin tungsten foil (or other metal foil made of single or polycrystalline materials [5]) with a few μm thickness, with as little defects as possible to keep the positrons from being trapped. To get rid of contamination and defects in the moderator material, an in-situ annealing procedure at high temperatures is necessary for most foils. [10] A moderation efficiency of 3×10^{-3} could be achieved with a single crystal moderator foil made of W. [11] A single crystal tungsten foil in a (100) orientation is used in the continuous positron beam of the VEPAS positron laboratory in Como.

A very high efficiency type of moderator is obtained by depositing a thin layer of krypton or neon on a carrier foil at low temperatures. [12]. These rare gas solid moderators have a small, positive work function, allowing only positrons with a kinetic energy larger than the workfunction to be emitted from the surface. Rare gas solid moderators show a slow thermalization process for e^+, which leads to a larger energy spread of emitted positrons when compared to metal

[5] Polycrystalline materials are substantially cheaper and easier to produce than single crystal moderators. Since they contain grain boundaries and defects, a large quantity of the positrons are trapped in the material and can not reach the surface.

foil moderators. This is compensated by the much higher efficiency of solid gas moderators. The very high efficiency of 10^{-2} has so far not been completely explained but is suspected to be due to a drift caused by an internal electric field, affecting the motion of the positrons.[13] For this type of moderator, a thin film of gas is frozen onto the source holder and can be renewed by evaporating the old layer and growing a new one. This process requires cryogenic appliances and vacuum systems. [7] A solid neon moderator is used in the AEgIS positron system at CERN.

Another possibility for future positron moderation is the use of a field assisted moderator made of SiC, the only known semiconductor with a negative work function. [14]

1.3 Trapping and Cooling of Positrons

Unlike for some experiments like the Doppler Broadening technique where a relatively small number of positrons arriving on the target directly from the source suffices, a much larger number of positrons is required for other experiments. This can be achieved through using a stronger positron source, which is often quite complicated, expensive and which only allows the increase to a certain extend. Therefore, an accumulator is used between the source and target region, which uses electric and magnetic fields to trap positrons. The basic principle is to collect the positrons from the continuous source and to store them for a certain time. Then all the collected positrons are released in a single positron dump. Since the positron beam forms a none-neutral compressed plasma (with non zero total charge) it can not be confined for an infinite time due to experimentally caused asymmetries in the electric and magnetic field. Therefore, the plasma expands radially and axially which has a negative influence on the positron lifetime. This can be counteracted by the use of Penning traps and the Rotating Wall technique.[15] These techniques don't only enable compression but also

cooling of the positron plasma. The trap used in the AEgIS-experiment is called a Penning-Malmberg trap.

The rotating wall principle improves the positron lifetime significantly and reduces the dimensions of the positron cloud, though not all the mechanisms for the rotating wall technique have been completely understood up to this point.

1.4 Positronium

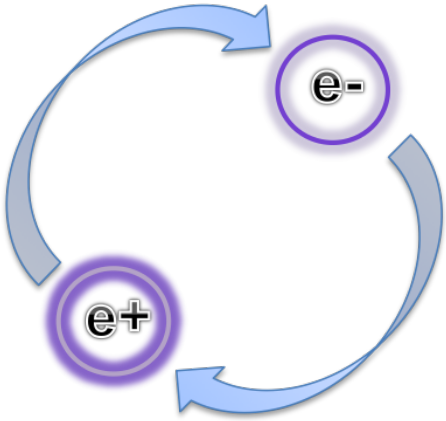

Figure 1.3: Positronium-Atom: The bound state of a positron and an electron

Positronium (Ps) is the quasi-stable bound system of an electron and its antiparticle the positron (e^+) and forms a purely leptonic atom (exotic atom), see figure 1.3. It was discovered by Deutsch in 1951 and has since then been the subject of many experimental and theoretical investigations.[16]

In vacuum and in its ground state (n=1), Ps can exist in two configurations, depending on the spin orientation of the e^+ and e^-:

- Parapositronium (p-Ps) in the singlet state (total spin 0, formation probability 1/4). In vacuum p-Ps decays into 2 γ-rays with an energy of 511 keV each and with a mean lifetime of 125 ps.

- Orthopositronium (o-Ps) in the triplet state (total spin 1, formation probability 3/4). O-Ps decays into 3 γ-rays with a total energy of 1022 keV, which is randomly divided between the 3 photons and with a mean lifetime of 142 ns.

Ps can be created by implanting positrons with an energy of a few keV into a particular solid target. [17] Due to its relatively long lifetime, o-Ps formed in materials with a network of connected open-volume defects can diffuse for hundreds of nanometers and eventually reach the surface where it can be emitted into the vacuum. [18]

There are two distinctive processes for positronium formation: Bulk formation and surface formation:

Ps Bulk Formation

In the case of Ps bulk formation in porous materials, the formation of Positronium is energetically more favorable than for the positron to stay as a separate particle. The formed Ps atom can annihilate or diffuse back to the surface and can be emitted due to a negative work function.
The positronium formed in the bulk diffuses in the material and if not trapped in voids or defects, can be emitted from the surface into the vacuum. [19]

Ps Surface Formation

When positrons leave the surface of a material they can bind to an electron and be emitted into the vacuum as positronium with a relatively high energy of a few eV.

Positronium formation in metals, semiconductor and insulators

The formation of Positronium depends on the target material and differs for metals, semiconductors and insulators due to their different densities of free electrons.

For metals, no formation of Ps in the bulk is possible, due to their high density of free electrons. This decreases the binding energy, to a level where Ps formation is no longer possible. The free electrons in the metal screen the Coulomb attraction between the positrons and any single electron. Due to a high number of surface states in metals, the probability for surface formation of Ps is higher.

For insulators, positronium is mostly formed in the bulk by thermalised positrons due to a low density of free electrons but this also lowers the cross section for an interaction between the positron and electron. Due to a longer thermalization time for positrons in insulators, a fraction of the positrons with sufficiently high kinetic energy can reach the surface by diffusion and form positronium even though there are only few surface states in which the Ps could form.

The Positronium conversion yield is especially high for SiO_2 with 72% in the bulk and 12% on the surface and may currently be the best known positron-positronium converter. [19]

1.5 Detectors

The detection of positrons and positronium is achieved through the detection of γ-rays, that are emitted during the annihilation process. In the AEgIS Positron system, a variety of detectors were used in the course of this thesis, to measure positron and positronium annihilations and to assess beam characteristics. Therefore several photon detectors (scintillating material) coupled to photo multiplier tubes or photo diodes were used, tested and compared. The spatial dimensions of the beam spot were characterized with an MCP (Microchannel Plate) assembly. In the VEPAS positron system a high-precision germanium detector was used for the detection of γ-rays.

1.5.1 Plastic or Crystal Scintillators

These radiation detectors are made up of two main components: The radiation converter and the detector. The converters are scintillating materials like a CsI crystal or a plastic scintillator, both of which are used in the AEgIS positron system. The electrons in the scintillator material are excited by the incoming high-energy photons and reemit this surplus energy when returning to their ground state in the form of low-energy photons (visible light). Depending on the material the above described process can take a few nanoseconds to tens of nanoseconds. Each incoming photon with enough energy is converted without additional filters added. Therefore it is necessary to place the detector close to the target with proper shielding to reduce the background noise and to perform a calibration for absolute numbers.

Different crystals can be used and can generally be divided into two groups: Inorganic (CsI, $PbWO_4$) and organic (Plastic). The inorganic crystals have a slower re-emission time than Plastic scintillators and are therefore slower but offer a higher quantum efficiency, with nearly every incoming high-energy photon producing many emitted low-energy photons. Some plastic scintillators show delayed fluorescence, resulting in an afterglow of the measured signal and a second component in the signal that is several tens of ns long. They show a low efficiency due to their low material density, causing many gamma rays to go through the detector without causing scintillation.

The converted low energy photons are then detected by a photo multiplier tube (PMT) or photo diode. Their functional principle is based on the photoelectric effect, transforming the incoming low-energy photons provided by the scintillator into electrons inside of a metallic photo cathode. The electrons are then accelerated by a high voltage towards several dynodes, producing secondary electrons and thereby amplifying the signal. This process requires tens of nanoseconds, producing a signal with a pulse width of a few ns. The produced voltage signal is proportional to the energy and number of incoming photons, see figure 1.4.

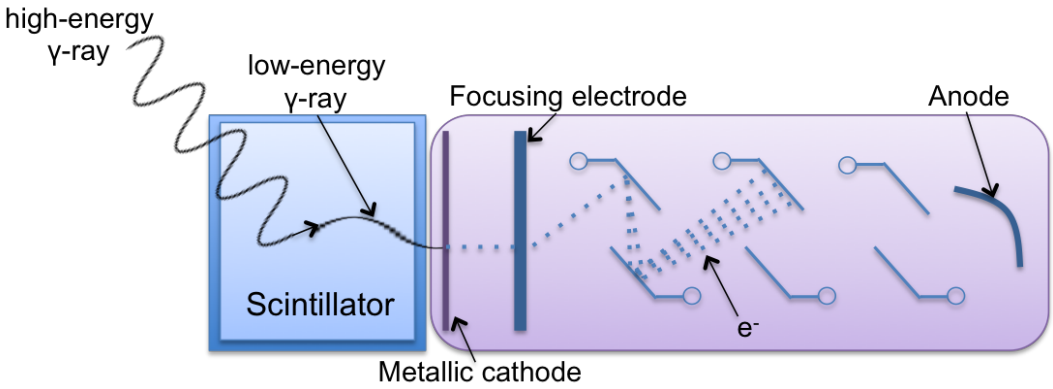

Figure 1.4: Basic working principle of a PMT coupled to a scintillator. High-energy photons are converted to low energy-photons, which hit a metallic cathode and produce a small current of electrons. These e^- are accelerated towards several dynodes, producing secondary electrons and resulting in an avalanche of e^-.

The photo diodes are also based on the photoelectric effect, creating a small current in the p-n junction of the diode. The more photons hit the Si diode the more the current increases (restricted by a resistor and a capacitor). Thereby a slowly decreasing signal (over several milliseconds) is created. Information about the total number of incoming γ-rays within a short time range can be obtained through the peak voltage. The biggest advantage of this type of detector is the insensitivity with respect to magnetic fields. A quite small detector unit is formed when coupled to a CsI crystal scintillator, which enables it to be moved around easily. [20]

1.5.2 Cherenkov Radiators

The Lead (II) fluoride (PbF_2) detector used during this thesis is a so called Cherenkov radiator. For this kind of material, with a high atomic number and with high density, no scintillation as described above can be detected. In contrast to scintillators, the method of this detector is based on pair production. The incoming high-energy photons hit the PbF_2 crystal and ionize the atoms of the material.

If this is the case, the deceleration of the charged particles produces the so called

Cherenkov light. The disadvantages of using these Cherenkov radiation based detectors, is the requirement for high-energy photons as input. Nevertheless it is possible to detect lower energy γ-rays, but the produced free electrons will consequently also have lower energy and only little Cherenkov light will be produced. Also the Cherenkov crystals exhibit a much lower quantum efficiency as compared to scintillating materials, since only a few photons are emitted for each incoming photon. In spite of this disadvantage the PbF_2 crystal based detector is still a suitable choice for positronium lifetime spectroscopy, see chapter 3.1. It offers an improved signal-to-noise ratio for the detection of positrons due to the property of only detecting high-energy photons. Because Cherenkov light is emitted instantaneously, they possess a very good temporal resolution. The PbF_2 Cherenkov radiator is, just like the scintillators, coupled to a PMT to enhance the low output. [21]

1.5.3 Multi-Channel Plate and Phosphor Screen

For beam characterization, a multi-channel plate (MCP) coupled to a phosphorous screen can be used. The working principle of the MCP is similar to that of the PMT, secondary e^- are used for amplification.
It is made of angled channeltrons with a diameter of a few μm. This small channels are placed side by side to form the MCP and are made of a material with high resistivity, emitting secondary e^- when hit by the positron annihilation photons. By applying a high voltage, the electrons are accelerated toward the end of the channels. Due to the angle of the channeltrons, the e^- eventually hit the walls of the channels, producing more secondary electrons, working as an amplifier for the signal. The electrons are further accelerated towards onto the phosphor screen, exciting the material and emitting light which can then be imaged by a CCD-camera. [22]

1.5.4 Semiconductor Detector

Like the above described photo diode, a semiconductor detector consists of a semiconductor usually made of Silicon or Germanium to measure the incoming photons of positron electron annihilation events. The high-energy photons generate charge carriers inside of the detector material, producing electrons and holes. An applied electric field accelerates electrons and holes to the electrodes, creating a pulse that can be measured. A fixed energy is required to create an electron-hole pair and does not depend on the energy of the incoming photons. Therefore the signal is proportional to the number of incoming photons.

In this thesis a high-purity Germanium detector is used, cooled with liquid nitrogen. Intrinsic Germanium at these low temperatures has an empty conduction band and consequently a high resistivity. When a photon hits the detector, a number of e^- proportional to the energy of the incoming photon is transported to the valence band. These kind of detectors offer an excellent energy resolution for γ-rays, superior to scintillators discussed above. [23]

1.6 Measuring methods of e^+e^--annihilation

In order to observe positrons and positronium, different techniques are used, based on detecting γ-rays produced through annihilation. The Single-Shot Positron Lifetime Spectroscopy technique was used for the measurements at the AEgIS positron system at CERN, the Doppler Broadening technique and positronium spectroscopy were used at the VEPAS system in Como.

1.6.1 Positron annihilation lifetime spectroscopy

Positron annihilation lifetime spectroscopy (PALS) is the most commonly used technique for the measurement of positrons inside of different materials, also pro-

viding information about positronium formation. When a positron is implanted into a material with a certain energy, it diffuses through the material, thermalizes and eventually annihilates with an electron inside the sample. A photon with an energy of about 511 keV is emitted. Single positrons are implanted into the sample and the annihilation time is measured with respect to a start signal. This is repeated until good statistical values are reached. Positron annihilations can be distinguished from ortho-positronium annihilations due to the elongated lifetime of the Ps-atoms. Usually, a gamma ray emitted simultaneously with the positron by the radioactive source is used as a start signal. The lifetime can be calculated based on this signal and the annihilation signal recorded by the detector. The lifetime depends on the investigated material and is proportional to its electronic density. The e^+ can get trapped in open volumes, like vacancies or cavities, and prolong the measured lifetime. The positron lifetime component increases with the size of the free volume and the intensity is proportional to the concentration of open volumes. [24]

1.6.2 PALS with pulsed e^+ beam

PALS with a pulsed positron beam, quoted in the following as Single-Shot Positron Lifetime Spectroscopy (SSPALS) is a similar technique as PALS discussed above, but involving the simultaneous presence of many positrons in the target, which is achieved through a pulsed positron beam. As a consequence it offers a much shorter collection time and is more suitable for depth profiling. Moreover it offers the possibility to study the simultaneous production of many Ps atoms, their interaction and their laser excitation. A disadvantage is the typically worse time resolution and the more complex experimental setup which is necessary to produce positron pulses and dump them with very accurate timing. For SSPALS a large bunch of positrons hits the target at the same time, with the dump of the positron cloud acting as the start signal. Like the PALS method, SSPALS offers the possibility to measure in different depths of the sample and study defects in different layers.

1.6.3 Doppler Broadening Spectroscopy

The Doppler Broadening Method is based on the detection of annihilation gamma rays and calculating the momentum of the electrons from the energy distribution of these photons, see figure 1.5. The momentum offers information about the electronic structure of the sample and the embedded defects of the material. Doppler Broadening spectroscopy can be performed with the sample placed directly in front of a radioactive source or, as was done for the measurements of this thesis, by using a continuous slow positron beam. When a positron annihilates with an electron of the material, a Doppler shift of the emitted photon can be measured due to the momentum of the electron involved in the annihilation process. The momentum of the positron can be neglected due to the thermalization process it experienced before the annihilation.

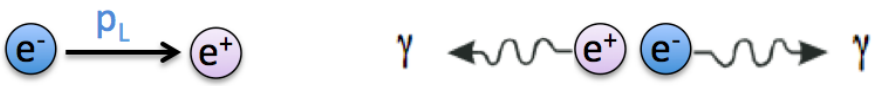

Figure 1.5: Schematic representation of an annihilation event of a e^+ and an e^-, giving rise to two 511 keV photons in two opposite directions.The recorded signal is Doppler-sensitive to the longitudinal momentum of the electron, the momentum of the thermalized positron can be neglected. The annihilation energy of 511 keV gets Doppler shifted by an amount E. Since many annihilation events are measured, the energy line is broadened due to the different Doppler shifts along the annihilation direction.

For the non-relativistic consideration the energy shift amounts to:

$$\Delta E = \frac{c}{2} p_L \tag{1.2}$$

p_L . . . Longitudinal component of the electron momentum

c . . . speed of light

The energy peak of the annihilated γ-rays is broadened around 511 keV due to the different momenta of the electrons inside the material, with which the positrons annihilate. Low momentum electrons (valence electrons) produce a

small energy shift, high momentum electrons (core electrons) produce a large energy shift.

This broadened peak is characterized by the two Doppler-parameters, called the S and W parameters and are characterized by the areas in figure 1.6.

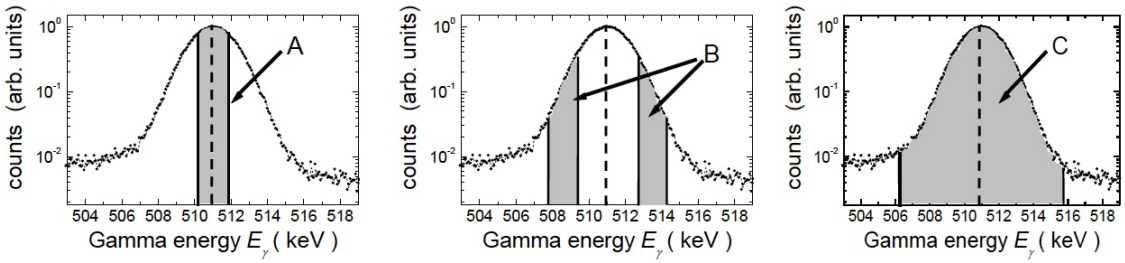

Figure 1.6: Characterizing areas of the broadened positron annihilation peaks to define the Doppler-parameters S and W adopted from [25]

The S parameter is defined as the count ratio in the central area (area A) and the total peak area (C).

$$S = \frac{A}{C} \tag{1.3}$$

The W parameter is given by the count ratio of the side regions (B) and the total peak area (C).

$$W = \frac{B}{C} \tag{1.4}$$

For this thesis the area A is defined as $|\ E_\gamma$ - 511 keV $|\ <$ 0,85 keV and the side areas B are defined as 2,75 keV $<|\ E_\gamma$ - 511 keV $|\ <$ 4 keV.
The total peak area C is given by (511 keV - 4.25 keV) $< E_\gamma <$ (511 keV + 4.25 keV).

The shape parameters characterize the annihilation peak.

For a narrow annihilation peak, a high value of the S parameter is obtained. In this case positrons annihilate with low momentum electrons (valence e^-). In open-volume defects there are more valence electrons than core electrons, annihilations of positrons trapped in these defects lead to a high value of the S parameter, then in materials with no defects. For a broad annihilation peak, a high value of the W parameter is obtained, the positrons annihilate mainly with high momentum electrons (core e^-). The sensitivity to open-volume defects makes Doppler Broadening spectroscopy a suitable tool to study defects in different materials and at varying depths of the material by changing the positron implantation energy. This enables the production of defect depth profiles of the investigated sample.[25] The advantage of Doppler broadening spectroscopy is that only the annihilation γ ray has to be measured, the measurement of a start signal is not necessary, therefore the method is faster.

The physical information contained in the parameter S(E) is obtained via fit programs. It uses the experimental values of the S parameter at the different positron implantation energies. The program used in this thesis is called VEPFIT.[26] It is based on the numeric resolution of the stationary diffusion equation and allows to evaluate the different properties of the investigated sample, like different materials, porous structures etc. The positron diffusion length can be determined as well as information on the inner boundaries.

1.6.4 Ortho-Positronium Spectroscopy

Ortho-Positronium Spectroscopy offers information about the average size and distribution of pores and their connectivity to the vacuum. For this technique the annihilations between an electron and a positron forming positronium are used. When o-Ps is formed, the annihilation process occurs into 3 γ-rays as opposed to 2 γ-rays for para-positronium formation. The emitted photons involved in the annihilation of o-Ps have an energy between 0 - 511 kV and result in an energy distribution illustrated in figure 1.7.

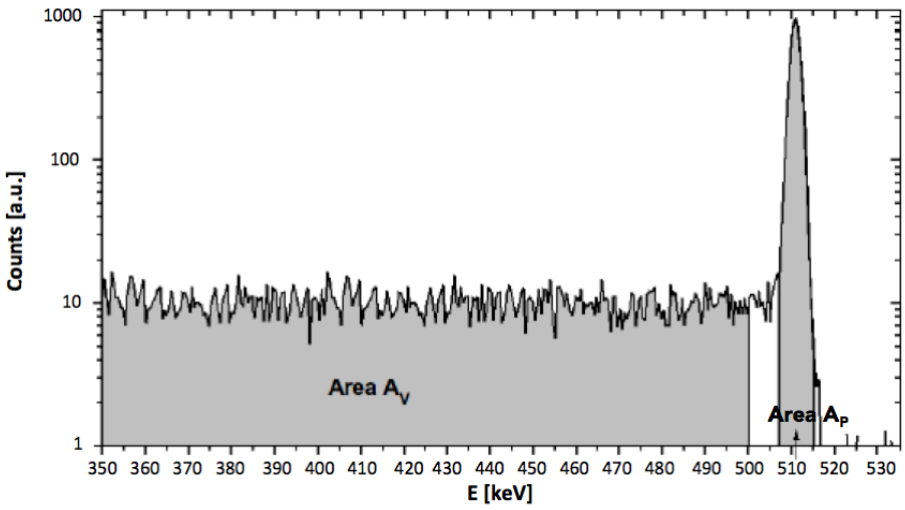

Figure 1.7: Positronium annihilation spectrum: Valley area containing 3 γ annihilations (A_V) and peak area containing 2 γ annihilations (A_P), for the definition of the R parameter adopted from [27]

It consists of a valley area (A_V) and a peak area (A_P), their ratio gives the so called R parameter.

$$R = \frac{A_V}{A_P} \tag{1.5}$$

For this thesis, the valley area was defined between an energy of 350 keV $< E_\gamma <$ 500 keV and the peak area at an energy of (511 keV - 4.25 keV) $< E_\gamma <$ (511 keV + 4.25 keV)

It is not easy to determine the total o-Ps yield, since both pick-off 2γ annihilation of o-Ps and annihilation of p-Ps can contribute to the 511 keV peak. Pick-off annihilation is a process where the positron bound in the positronium atom, doesn't annihilate with the bound electron with parallel spin, but annihilates with an other electron of the material with anti-parallel spin. The Ps atom then annihilates into 2 γ-rays instead of three and contributes to the peak area instead of the valley area, with a lifetime reduced to para-Ps lifetime compared to ns for 3 γ annihilation. Only upon escaping of the Ps atom from the surface, there is no possibility for pick-off annihilation and all o-Ps atoms annihilate into 3 γ-rays.

Therefore, on the surface the total o-Ps fraction $F_{3\gamma}$ can be calculated without losses from pick-off annihilation, see chapter 3.3.2.

1.7 Laser excitation

To prolong the lifetime for anithydrogen production, the positronium atoms are excited to Rydberg levels. Rydberg states are electronically excited states with a quantum number of n>10 and can be compared to the excited states of hydrogen atoms, replacing the proton of the hydrogen core with a positron. The excited stages are reached with the help of a short laser pulse in the order of ns, exciting the produced Ps atoms at emission into the vacuum.

The required energy to excite Ps atoms to Rydberg levels from the ground state is approximately 6.7 eV. With the current technologies it is not possible to directly excite Ps from the ground state to Rydberg states, since a UV laser with a wavelength of about 180 nm would be needed. Instead it is achieved in two steps, exciting positronium with two laser pulses with different wavelengths.

The produced Ps-atoms are therefore excited to lower excited states (n=2 or n=3) by a UV laser and then excited further to Rydberg states by an IR laser. The Ps Rydberg excitation has been achieved by Cassidy and co. [28], the transition over the n=3 state was first achieved by the AEgIS collaboration during the time of this thesis and was submitted to be published in October 2015. [29]

The excitation process is achieved by means of absorption of incoming photons of the UV laser beam, by the o-Ps atoms.

$$o - Ps + \gamma_{UV} \rightarrow o - Ps^* \tag{1.6}$$

2 Experimental Setup

This chapter discusses the experimental setups of the facilities used for the measurements conducted during this thesis.The experimental work took place at the AEgIS experiment and at the slow positron beam of the VEPAS group in Como/Italy. Described are the individual elements and different modules for e^+ and Ps experiments and the surrounding apparatus.

2.1 CERN and the AEgIS-Experiment

The AEgIS collaboration was founded in 2007 and is the successor of an earlier antimatter experiment called ATHENA, whose goal was the production of anti-hydrogen. The main objective of the AEgIS experiment is the direct measurement of the effect of the earths gravitational acceleration on antimatter, more precisely on antihydrogen. Currently the experiment is working on the production of antihydrogen and is still in the starting phase of its discoveries. The AEgIS collaboration is divided into small groups focusing on different parts of the experiment and all combining their expertise when the experiment is running. It is located at the CERN facilities in Geneva/Switzerland, in the Antiproton-Decelerator-Hall, where AEgIS and other antimatter experiments receive antiprotons from the antiproton-decelerator ring. The AEgIS-Experimental-Setup consists of three main parts:

- The main magnets region with the purpose of antihydrogen production and gravitational measurements.
- The Positron system, with the purpose of providing a positron beam to an experimental chamber or to the main magnets region.

- The laser system for Rydberg excitation of positronium delivering laser pulses to the main magnets region and the positron system.

2.1.1 Production of antihydrogen

The concept for the measurement of the effect of the earths gravitational acceleration on antihydrogen is outlined in figure 2.1.

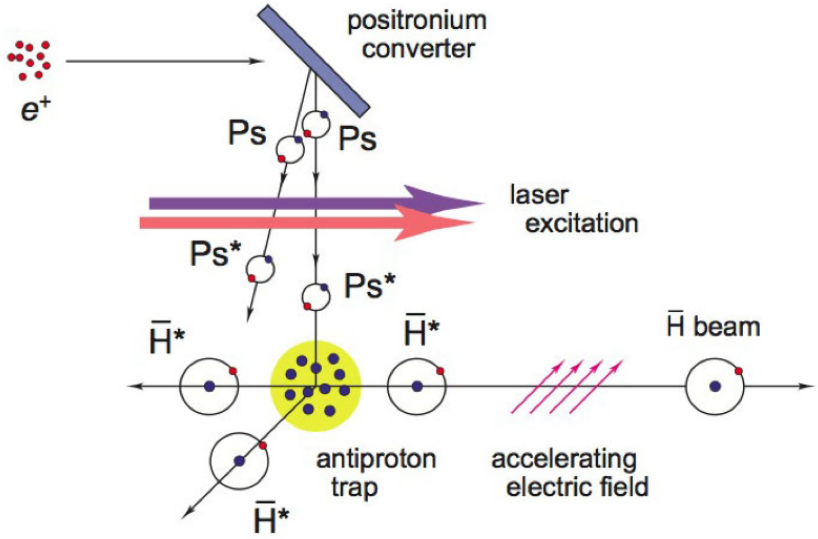

Figure 2.1: Outline of the basic principle for the measurement of the effect of gravity on antihydrogen at the AEgIS experiment. A e^+ bunch is directed onto a e^+/Ps converter, the formed positronium is excited to Rydberg states through a 2-step laser system. The Ps* atoms and antiprotons are combined to form $\overline{H}^*$ and formed into an $\overline{H}^*$ beam. [30]

The first step is the production of positronium by injecting positrons into the main magnets region and guiding them onto a special porous Silicon target where they form positronium.

The Ps-atoms are then excited to Rydberg states by a laser system and combined with the antiprotons from the antimatter decelerator. Thereby excited anithydrogen atoms are formed through charge-exchange reactions between the $\overline{p}$ and Rydberg-excited Ps and can then be accelerated through an electric field via

Stark acceleration. An $\overline{H}$ beam is obtained, which finally passes through a moiré deflectometer to measure the effect of gravity on the antihydrogen atoms by measuring their vertical displacement after the pass-through.
This deflectometer is made up of successive gratings, followed by a detector sensitive to the position of the $\overline{H}$ (e.g. pixel detectors).
Because the diameter of the apertures of the gratings exceed the de Broglie wavelength of the antihydrogen atoms, an interference pattern is formed by the atoms crossing through the gratings. [30]

2.1.2 Overview of the AEgIS Main Magnets Region

The AEgIS main magnets region is the heart of the experiment and the place where antihydrogen production and antigravity measurements take place. A simplified overview of the system is shown in figure 2.2.

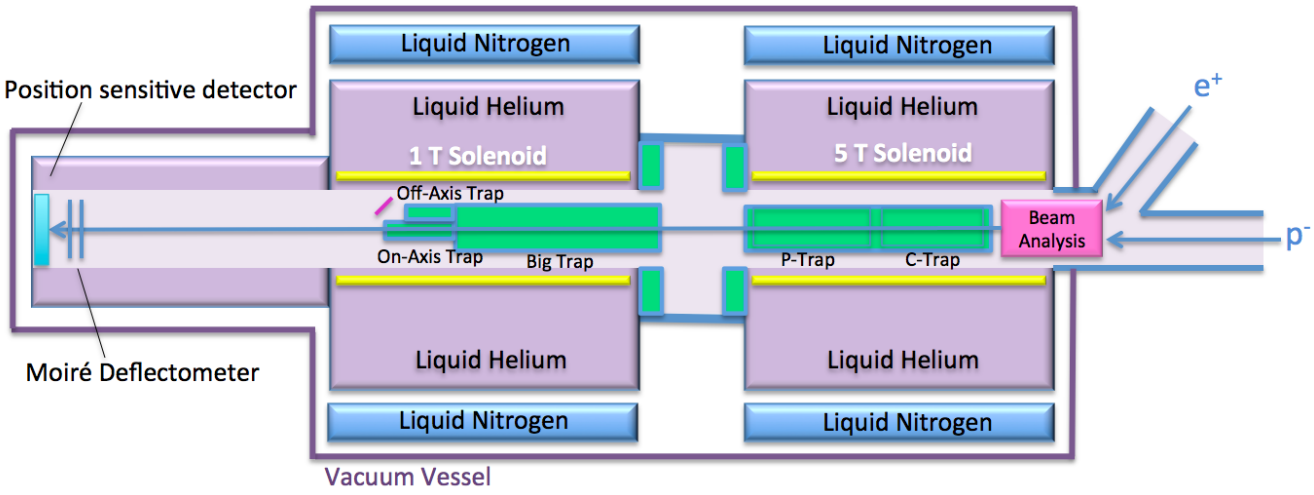

Figure 2.2: Overview over the cross section along the main axis of the main magnets region of the AEgIS apparatus with the different trap areas for positrons and antiprotons in the 5T and 1T regions.

The central element is the evacuated beam line (grey) which is surrounded by the 1T and 5T superconducting solenoid magnets (yellow). The superconducting magnets are cooled by liquid helium at 4 K surrounding the magnets (purple squares). The positron beam that arrives from the AEgIS positron system at 300

eV and the antiprotons arriving from the AD-Hall at 5 MeV enter the system and pass on into the 5T magnet used for catching and accumulating antiprotons and positrons. Since much lower magnetic fields are desired for particle manipulation and for the gravity measurement, antiprotons and e^+ are then transported into the 1T trap where they are compressed longitudinally and radially.

A positronium target is mounted at the end of the Off-Axis trap (pink) towards which the positron cloud will be accelerated to create Ps and be excited by a laser system to Rydberg states. In the final area, a moiré deflectometer [31] will be installed in the near future coupled with a position sensitive detector to measure the vertical displacement of antihydrogen.[32]

2.2 The AEgIS-Positron system

The AEgIS positron system is the main focus of this thesis and will be discussed in detail in this chapter. The different components of the system will be described, as well as their operational principles, a basic overview is shown in figure 2.3.

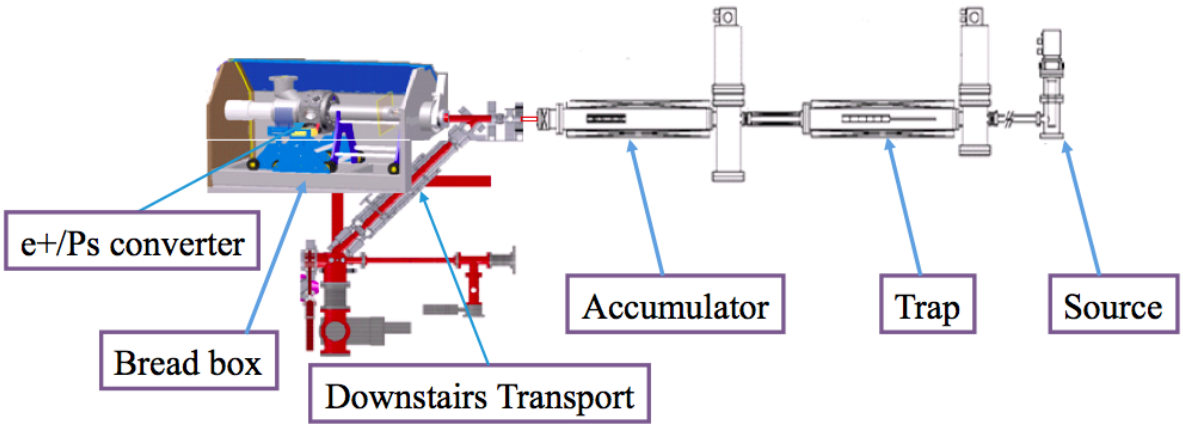

Figure 2.3: Schematic of the basic components of the AEgIS positron system and their arrangement. Detailed descriptions of the individual components can be found below.

2.2.1 System Overview

High vacuum conditions are necessary to be upheld inside the whole system, which is achieved through the use of a sequence of vacuum pumps (roughing, cryogenic and ion pumps). The different sections of the system are connected through pneumatic valves and can be separated when turning it off.

The positron system can roughly be divided into four parts:

- Source
- Accumulator
- Buncher
- Experimental chamber (Ps test chamber)

For antihydrogen production the positrons are transported to the main magnets region located downstairs, but the Ps test chamber was installed above the main system for additional measurements like the test of positronium targets and laser excitation in a potentially zero magnetic field environment. To transport positrons, electric and magnetic fields are used. To avoid overheating, all coils are water-cooled. To guide the e^+ into the main magnets region, an angle shaped solenoid is used to bend the positron beam. Prior to the entrance of the Ps test chamber the guiding system is switched from magnetic to electric to enable a zero magnetic field environment in the experimental chamber. Each element in figure 2.4, starting from the source on the right to the positron/positronium converter on the left will be described in detail below.

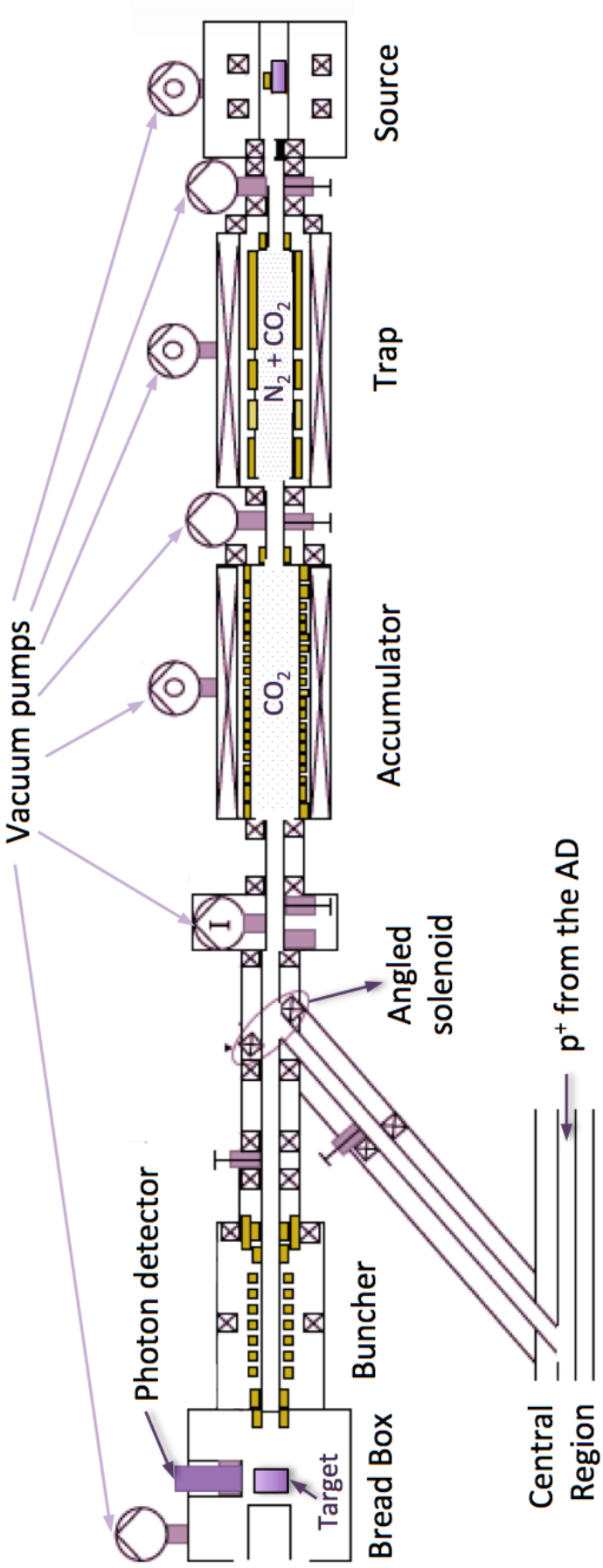

Figure 2.4: Overview over the the AEgIS positron system and its main components

2.2.2 ^{22}Na Source and Solid Neon Moderator

Since positrons are very light particles, they are sensitive to outer magnetic fields along the positron transfer line, especially around the source area. Therefore the magnetic field along the AEgIS positron system was measured at 4 different points and as a consequence μ-metal shielding was installed. This was done by the author during the time of this master thesis in the group of S.Mariazzi.

The positron source used at AEgIS is a ^{22}Na source. With a half-lifetime of 2.6 years for ^{22}Na and an initial activity of 21 mCi in 2011 the current activity level can be calculated to approximately 10 mCi or 370 MBq. In 89% of all decay events positrons are emitted, which amounts to approximately $3.3 * 10^8$ e^+ emitted per second. The complete source system was produced by First Point Scientific Inc., except for the ^{22}Na itself which was provided by a South African company called iThemba.

The β decay process is described as follows:

$$^{22}Na \longrightarrow {}^{22}Ne + e^+ + \gamma \tag{2.1}$$

The sodium source is embedded in walls made of tantalum, which due to its high atomic number is well suited, as it reflects the e^+. As a result of this setup, the positrons that form the beam are only the ones emitted towards the moderator or the ones that are backscattered in this direction. The complete source area is located inside of a lead shield for radiation protection, see figure 2.5.

The source is located in the vertex of a copper cup where a solid neon moderator is deposited. During this procedure the pressure in the source area is at 10^{-9} mbar, at which the neon gas solidifies at a temperature of 10 K. The moderator efficiency given by the manufacturing company First Point Scientific Inc. lies at $2,5 \cdot 10^{-3}$. Only a small fraction of positrons emitted towards the trap are moderated, due to the wide band gap of the neon moderator. Therefore a tungsten block is installed

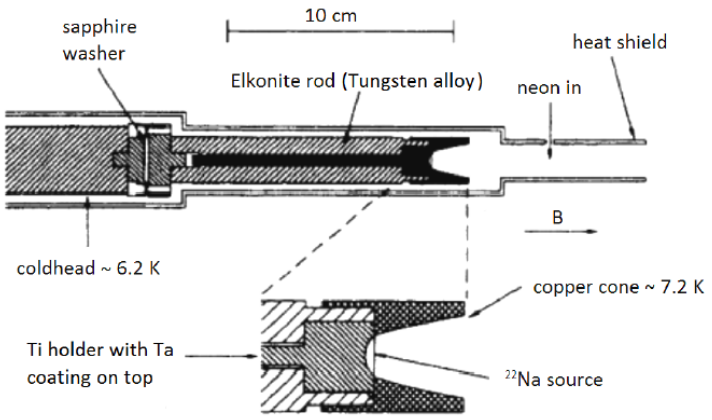

Figure 2.5: Layout of the e^+ source of the AEgIS positron system. The sodium is mounted on tantalum coated titanium holder. It is positioned inside an elkonite rod, which is electrically isolated by a sapphire washer and can be cooled down to approximately 7K. [33]

between the source and the trap that closes off the beamline. Two coils with opposite polarity produce a magnetic field to guide the positrons in the right energy range around the tungsten obstacle. Through this method the e^+ with the wrong energies can be filtered out and the tungsten block also functions as a shield for gamma radiation coming from the source. The growing of a new moderator is automated and controlled through a LabVIEW program. This process takes approximately 40 minutes and is outlined below: The coldhead is switched off and the temperature increased to 25 K evaporating the solid neon layer on the copper cup, the excessive gas is exhausted via a roughing pump. The chamber is cooled down to 8.8K and new neon gas is injected. Due to the low temperatures it solidifies on the surface of the source. After an annealing time at 9.3K for 15 minutes for the removal of defects, the coldhead reaches 7K again. Because of the characteristics of the moderator the positron system is not used directly after growing a new moderator, to ensure a stable number of positrons for experiments continuing over several hours.

In the past the AEgIS experimental zone has proven to be a strongly magnetic environment both through AEgIS internal magnetic fields, and fields from the surrounding experiments. Since positrons are very sensitive and easily influenced,

shielding of the system, especially the source area, was necessary to obtain stable beam conditions throughout the measurements. Below the source a strong dipole magnet is located, stearing the antiprotons from the AD into the AEgIS main magnets region. When this magnet is turned on, severe positron losses were recorded. Therefore, during this thesis, extensive measurements of the magnetic environment of the AEgIS experimental zone were conducted. Subsequently a μ-metal shield was installed around the entire source area and the saddle coil, which has also proven to be sensitive to changes in the magnetic field. CsI detectors were installed along the beam line to be able to quickly locate the area along the beamline where the positrons are lost.

2.2.3 Positron Trap

The trap used in the AEgIS positron system is a Surko-type trap [34] combined with the rotating wall principle, see figure 2.6.

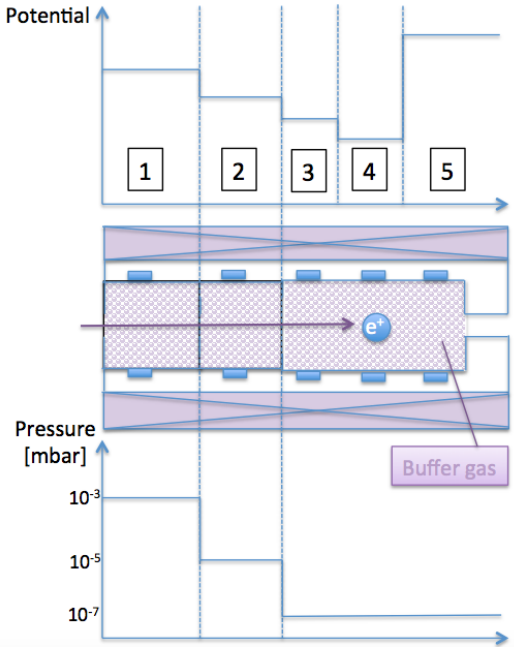

Figure 2.6: Schematic setup and working principle of a Surko-type trap, with Penning-Malmberg type of particle confinement. [35] The stepped potential for axial confinement and corresponding, gradually decreasing pressures can be seen, a longitudinal magnetic fields fends for radial confinement.

In the trap the e^+ arriving in a continuous positron beam from the source are collected and formed into an e^+ pulse. The trap is kept at a pressure of 10^{-10} mbar of and at 10^{-4} mbar during working mode, by the combination of a cryo and roughing pump. The enhanced pressure during operation arises from the buffer gas injection of 0.5 sccm/min of nitrogen and 0.03 sccm/min of carbon dioxide. Inside the trap a confining magnetic field of 0.07 T is used. Storage is achieved through six electrodes setting the step potentials and is modified in 3 stages with a reaction time in the order of 100 μs.

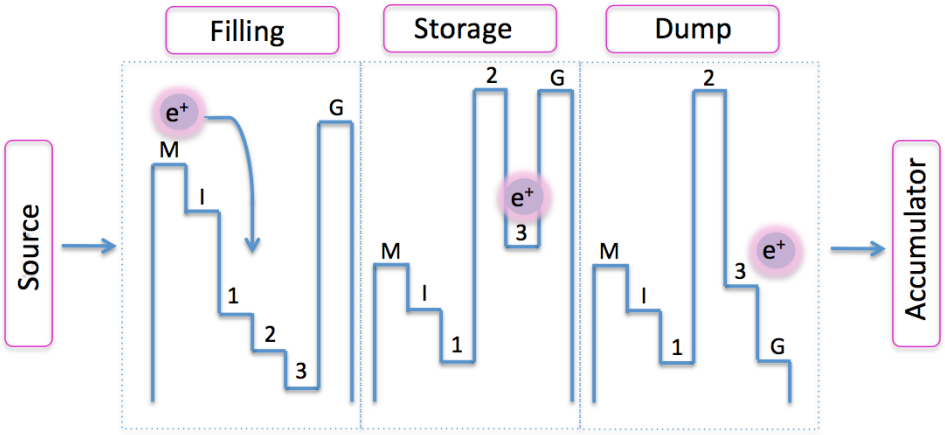

Figure 2.7: Outline of the positron storage process in the trap. The e^+ arrive from the source on the left and enter the trap in the filling stage. They loose energy through the buffer gas and are stopped by the Gate electrode (G). In the storage stage the e^+ are trapped between 2^{nd} and Gate electrode. In the dump stage e^+ are released into the direction of the accumulator.

The whole process takes 0.15 s and forms one positron pulse which is then transported to the accumulator. In the first stage e^+ enter the trap area, the inlet electrode (I) is set to a low potential to allow an easy entry of positrons from the source. Through inelastic collisions with the atoms of the buffer gas, they quickly lose energy and are stopped by the gate electrode (G) which is set at a high potential. Depending on their energy the e^+ are trapped between the 2nd and 3rd electrode. In the 2nd stage the potentials of these two electrodes are increased, creating a trapped positron pulse between the 2nd and gate electrode. In the 3rd and last stage the gate potential is lowered quickly, releasing the positrons into the direction of the accumulator. The transfer is done via magnetic transport

and achieved through a pair of coils and a permanent magnet to correct small misalignments.

2.2.4 Accumulator

From the trap the positrons are guided into another Surko-type trap combined with a rotating wall called the accumulator, with 6,5 e^+ pulses per second containing some 10^4 positrons, depending on the source intensity (declared by First Point Scientific Inc. and can be calculated from the positrons exiting the trap and considering the losses during the trapping process). In the accumulator the positron pulses from the trap are collected and compressed. The e^+ pulses can be released, when needed. Instead of a stepped potential, the 21 electrodes of the accumulator form a harmonic potential well which leads to efficient cooling of the positrons. As the cooling process takes place, the size of e^+ cloud is decreased longitudinally. Every 0.15 s a new positron pulse is added and up to several hundred positron pulses can be collected this way, offering a high number of accumulated e^+. The process of accumulating positrons is outlined in figure 2.8 and is done in 3 stages:

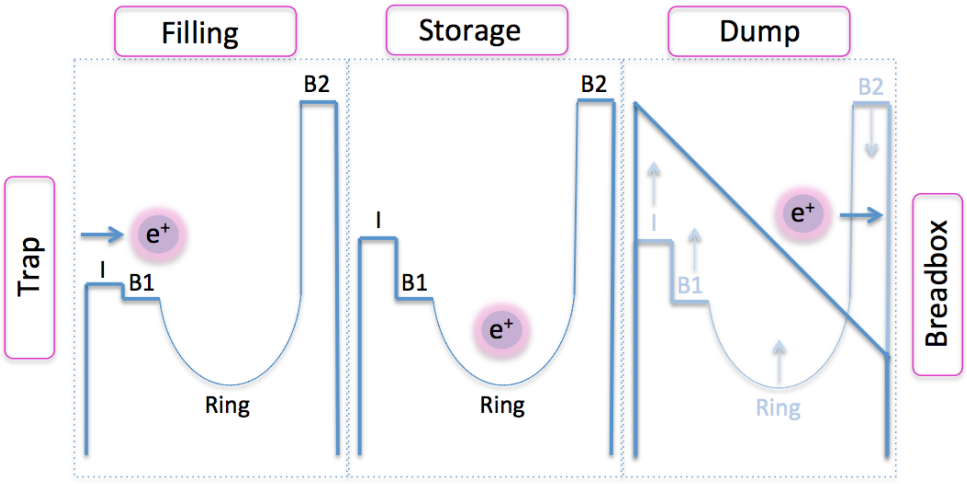

Figure 2.8: Outline of the positron storage process in the accumulator. In the Inlet (filling) stage e^+ pulses are arriving from the trap, in the accumulation (storage) stage the positrons are stored cooled and compressed and in the dumping stage they are released into the transferline in the direction of the Ps test chamber.

In the **Inlet stage** the positrons are admitted into the accumulator by lowering the inlet potential for every arriving pulse. In the **Accumulation stage** the e^+ are trapped in the harmonic potential and cooled through collisions with buffer gas atoms. The cooling efficiency is dependent on the number of positrons and decreases with the number of pulses accumulated. The number of positrons increases with the storage time, it is limited by the positron lifetime inside the accumulator. The last stage is the **Dumping stage** which is triggered by a signal to release the accumulated positrons from the accumulator into the transfer line.

After being dumped from the accumulator the positrons are transported via magnetic and electrostatic transport to the main magnets region or to the experimental chamber.

2.2.5 Buncher

The installation and implementation of the buncher was done by the author during the time of this thesis in the group of S. Mariazzi. As a part of the electrostatic transport a buncher has been installed to reduce the time spread of the positron bunch and accelerate them further towards the main magnets region. This bunching method previously has been used in other positron systems [36] and has shown a notable compression of the positron beam. The buncher of the AEgIS positron system is shielded by a μ-metal electrode, that marks the transition between magnetic and electrostatic transport (figure 2.9).

A parabolic potential between the first and last electrode is used to accelerate positrons arriving later (end of the cloud) more strongly than the ones arriving early (closer to the Ps test chamber), which reduces the time spread of the bunch. After the positrons pass through the buncher they reach the experimental chamber, where they are guided onto a a positron/positronium converter. The basic setup of the Ps test chamber can be seen in figure 2.9.
The positronium target is mounted on an actuator which is positioned perpendicular to the beam line (perpendicular to the drawing plane at the position of

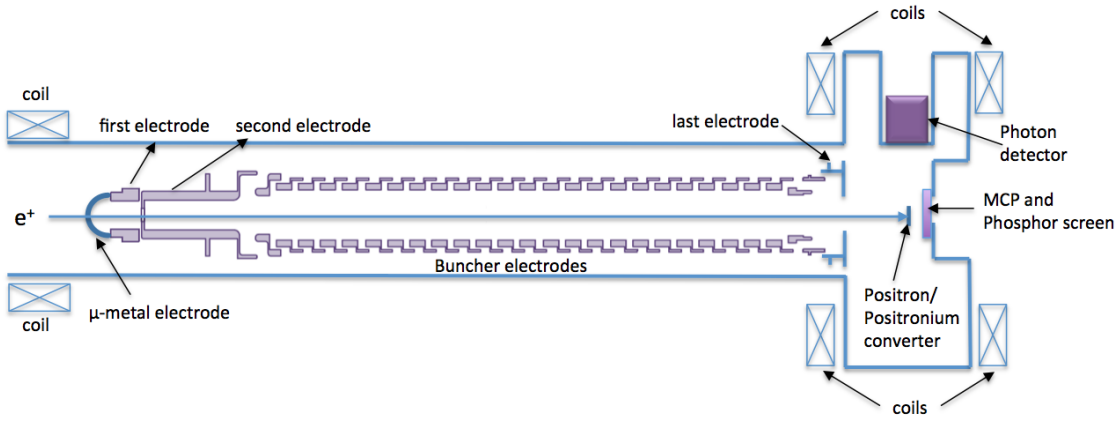

Figure 2.9: Outline of the buncher installed in the AEgIS positron system. The buncher is embedded into the positron transferline ending in the experimental chamber. The transport changes from magnetic to electrostatic at the μ metal coil after which the positrons enter the buncher from the left of the graph. They are accelerated and compressed and are guided into the Ps test chamber where they hit the positronium target.

the target). Up to three different samples can be fixed to it and the actuator can be removed from the beam line, for measurements with the MCP in the back of the chamber. Additionally the actuator can be positioned so that the e^+ hit the sample holder made of aluminium for background measurements.

Above the target a photon detector is placed for positron measurements, a viewport on the side of the experiment was installed for laser excitation of the produced positronium atoms.

The coils installed around the experiment produce a magnetic field inside of the main magnets region ranging between 2-300 Gauss for measurements in different magnetic environments.

2.2.6 Detection of Positrons/Positronium and System Calibrations

Several different detectors and detection methods are used inside the positron system to monitor the beam along the beam line and the experiments inside the Ps test chamber. In this chapter the function and position of these detectors are described. The different detectors of the Ps test chamber were installed and tested

by the author of this thesis in the group of S. Mariazzi.

Positron detection along the transferline

To monitor the beam along the beam line, two CsI photon converters coupled to a PMT are placed above the saddle coil (between the source and the trap) and behind the trap, see figure 2.3. These fast detectors permit to optimize the settings of the system between these two points by closing a vacuum valve after the trap and measuring the positron annihilations. The positron transfer is optimized with the lowest possible positron annihilation signal at the saddle coil and highest annihilation signal around the trap. Two CsI converters coupled to photodiodes are used for analysis of the bunched positron beam after the accumulator. The advantage of the photodiodes is that they are not sensitive to magnetic fields and their amplitude is proportional to the number of positrons contained in the dump but they are slower compared to the CsI-PMT couplings. The CsI-Photodiode couplings can be moved along the outer surface of the equipment due to their small size.

Positron/Positronium Detection in the Test Chamber

Other types of scintillators are also coupled to a PMT and installed above the experimental chamber in a cylindrical inlet about 3 cm from the target to maximize the solid angle, see figure 2.9. This setup is used to detect positron annihilations inside the experimental chamber and obtain life time spectra via SSPALS for positronium detection.

Different photon converters namely a Pilot U plastic scintillator (Height: 38 mm, diameter: 25 mm) and a crystal scintillator (Height: 20 mm, square base: 25 mm) made of $PbWO_4$ have been tested subsequently. A more detailed description of the detectors is given in chapter 1.5. Shielding is necessary for these scintillators,

since they detect photons at a range of different energies including stray photons from the experiment and cosmic radiation.

A PbF_2 Cherenkov radiator (Height: 60 mm, diameter: 20 mm) has also been used for a part of the measurements. The photon converters are coupled to a PMT H3378 and R11265-100 by Hamamatsu. The signal coming from the PMT is divided by a beam splitter (50 Ohm Mini-Circuits ZFRSC-2050B+) and sent to an oscilloscope (Tektronix TDS5054B, bandwidth: 500 MHz, resistance: 50 Ohm) [37]. The first channel with a gain of 1 V/div (vertical scale) is used to acquire the initial high-intensity signal peak of the annihilating e^+, the second channel with a gain of 100 mV/div records the low-intensity signal after the peak to reduce noise levels. The data acquired from the oscilloscope is automatically transferred to a computer and the two signals are combined to form SSPALS spectra.

A multi-channel plate (MCP) coupled to a phosphor screen is placed behind the target in order to characterize the e^+ beam and to obtain information about the geometry and intensity of the positron bunch reaching the MCP. The light emitted by the phosphor screen is imaged by a Hamamatsu ORCA-R2 digital CCD camera, model C10600-10B installed outside of the main magnets region behind the screen.

Calibration of the positron system

Both the CsI-Photodiode and CsI-PMT detectors have been calibrated to correlate the output signal to the number of annihilating positrons.

Calibration of the CsI-PMT: The first calibration has been done during the construction of the e^+ line and is necessary not only to receive a relative signal but to obtain the total number of positrons from the signal amplitude. The CsI-PMT was calibrated with a ^{22}Na source, that is not part of the AEgIS experiment. The total number of positrons emitted from the source was estimated and the detector was placed at a defined distance and solid angle from the source. The

obtained signal then corresponds to the number of positrons estimated for this specific distance and angle. The calibration was confirmed using a ^{133}Cs source and the same experimental method as described above.

Determination of transport and trapping efficiency: Later, the AEgIS ^{22}Na positron source was used with an activity of 21 mCi at the time of the calibration. The calibrated CsI-PMT was placed along the positron beam line before the trap in a specific distance behind a phosphor screen installed specifically for this purpose, see figure 2.9. All electrodes inside the trap were switched off and no buffer gas was injected, the positrons arriving from the trap are forced to annihilate on the screen. With the known number of positrons emitted from the source, the transport efficiency for positrons is calculated to $\sim 3 \cdot 10^{-3}$, which implies nearly perfect positron transport when compared to the moderator efficiency, see chapter 2.2.2. Since the number of positrons arriving at the trap was known ($2.3 \cdot 10^6$ e^+/s), the phosphorus screen was also calibrated and the correspondence between intensity of luminescence and number of positrons was obtained. The trapping efficiency was determined to 14% compared to 17% declared by the manufacturer First Point Scientific, then determined using the calibrated phosphor screen.

Calibration of the CsI-Photodiodes and determination of accumulator efficiency: The CsI photodiodes were also calibrated using this setup and were placed in certain distance from the phosphor screen before the target and at a specified solid angle, see figure 2.9 .

The accumulator efficiency was obtained through a calibrated CsI-photodiode with the same solid angle used for the calibration mentioned above placing it before and after the accumulator for comparison. No significant losses could be measured which suggests high efficiency of the accumulator. When 1000 pulses are accumulated with $1.1 * 10^4$ positrons per pulse, $1.1 * 10^7$ positrons can be expected at the exit of the accumulator which is supported by experimental results. Losses are negligible small, because very few annihilations with residual

gas atoms and the walls are expected due to the structure of the accumulator. The number of detected positrons is linear, for a doubled number of e^+, a signal of double height will be obtained, up to the level where the lifetime of positrons in the accumulator starts to saturate the curve, see figure 2.10.

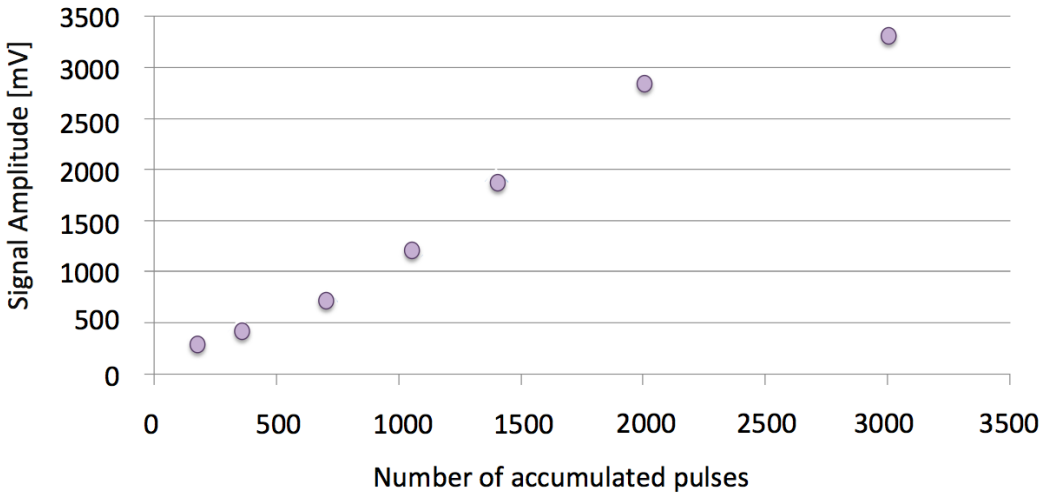

Figure 2.10: Signal amplitude over the number of pulses collected in the accumulator. The linear behavior of the detector is shown, for a doubled number of positrons a doubled signal is obtained. The saturation starting at around 2000 pulses suggests a misalignment of the accumulator. Due to this misalignment no optimal compression of the positron bunch can be achieved and from a certain number of e^+, annihilations with the walls of the accumulator occur.

The read out of the CsI detectors can be achieved directly over LabVIEW programs controlling the system. This offers an overview of positron annihilations along the entire positron system by moving the CsI detectors. 5 more of these detectors have been ordered to be installed along the experiment to provide instant access to information about positron losses at all relevant points of the system. The positron dump from the accumulator is also controlled through a LabVIEW program, which additionally offers an overview of all vacuum pump states, pressures and temperatures. If any of the monitored values deviates from its normal state, a warning appears inside of the program and an error message is sent to the users.

2.3 The AEgIS Laser System

For antihydrogen production in the AEgIS experiment positronium atoms and antiprotons will be combined.

$$Ps^* + \overline{p} \longrightarrow \overline{H}^* + e^- \tag{2.2}$$

Unlike in other similar experiments producing antihydrogen, the AEgIS experiment plans to use this method instead of simply mixing positrons and antiprotons. Working with positronium offers advantages over using isolated positrons: The positronium atoms can be excited to Rydberg levels, which permits the production of Rydberg excited anithydrogen atoms. Due to the dependence of the positronium lifetime on the quantum number n, proportional to n^3, the lifetime of Ps can be significantly increased through the laser excitation. Positronium atoms in Rydberg states also exhibit a large cross section for antihydrogen production with antiprotons in the order of 10^{-8} cm^2, because the cross section is expected to be proportional to n^4. [2] A further advantage is the possibility to produce very cold antihydrogen atoms in the order of 25-80 m/s, since less energy is introduced by mixing antiprotons with the neutral positronium atoms. Moreover, from antihydrogen produced in a Rydberg state, antihydrogen beams can be generated by using electric field gradients in the main magnets region.

The Rydberg excitation described in chapter 1.7 has so far been successfully tested in the main magnets region and is carried out in two essential steps: In the first step the Ps-atoms are excited into the n=3 state and in the second further to Rydberg states of n>20. The transition energy from the groundstate to the Rydberg state is greater than 6 eV. This high transition energy requires a two step laser excitation, since lasers with an energy of more than 6 eV do not exist yet. The Ps excitation to Rydberg levels was previously achieved by other experiments through exciting to the n=2 state and then to n>20, but the excitation through the n=3 level has never been performed so far. The excitation beyond over n=3

requires less power, therefore Rydberg excitation is favoured over ionization of the Ps atoms. When positronium is ionized the electron and positron are separated and the e^+ quickly annihilates. With the n=3 transition, ionization and the fast decay of the n=2 level is avoided.

For Ps excitation to the n=3 state a wavelength of 205 nm is needed, to further excite to Rydberg levels a wavelength of approximately 1670 nm is required depending on the number of the Rydberg level. This is achieved through two separate laser pulses, starting with a UV-laser pulse tunable between 204 and 206 nm with a pulse time length of 1.5 ns, a bandwidth of 150 GHz and an energy of 60 μJ. The second laser pulse, an IR-laser pulse with a length of 4 ns and an energy up to 55 mJ, excites the Ps atoms from n=3 to Rydberg levels. A scheme of the laser excitation process can be seen in figure 2.11. Both laser pulses are created by a Q-switched Nd:Yag laser.

The laser pulses are superimposed in space and time and transported to the experimental chamber by the same optical system. A separate transport system is implemented for transport to the main magnets region. A paper about Ps excitation to the n=3 state was submitted for publication by the AEgIS collaboration during the time of this thesis. [29] See [38] for a detailed description of the AEgIS laser system.

2.3.1 Detection of excited Positronium Atoms

The n=3 Ps^* atoms can be detected via magnetic quenching of the excited state or by photo ionization of the excited positronium atoms using a dedicated laser pulse. Magnetic quenching denotes the fact that a magnetic field induces a decay of the s=1 excited state of the Ps atoms to the s=0 ground state. This para-Ps ground state is associated with a much shorter lifetime of 125 ps, compared to 142 ns for non-excited ortho-positronium atoms that are not quenched. By means of photo ionization, the bond between the e^- and e^+ in the n=3 excited Ps^* states is broken, which gives rise to quick e^+ annihilation, i.e., a reduced e^+ lifetime.

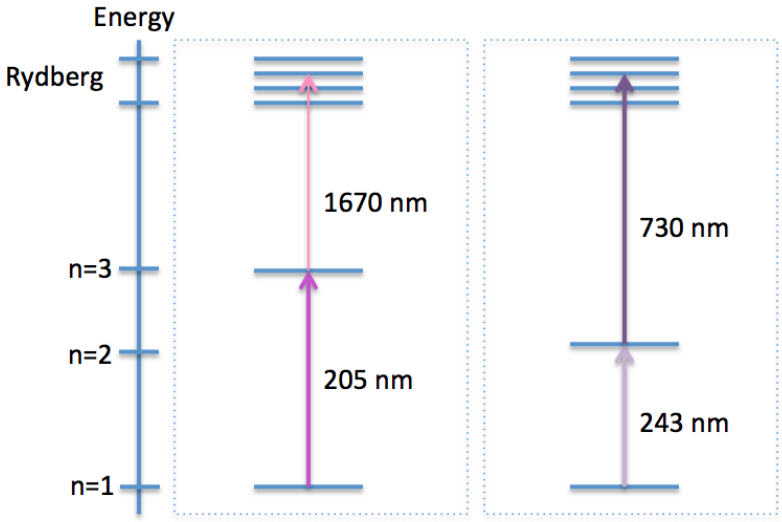

Figure 2.11: Outline of the laser excitation process, where two possibilities for transition to Rydberg states are shown: The transition used at the AEgIS experiment from n=1 to n=3 with a 205 nm pulse and from n=3 to Rydberg states with a 1670 nm pulse is presented on the left. On the right the transition from n=1 to n=2 via a 243 nm pulse is shown and from n=2 to Rydberg states with a pulse of 730 nm.

To detect Rydberg excitation, the change in lifetime is compared in the recorded SSPALS spectra. The prolonged lifetime of Ps^* is visible in the spectra as a long time constant exceeding 142 ns. This can be explained through the Ps^* atoms travelling through the vacuum until they reach the walls of the Ps test chamber and annihilate. For each of the methods described, the two laser beams applied for the generation of Ps^* are switched on/off for every second measurement inside the Ps test chamber and a comparison of both lifetime spectra is made.

2.4 VEPAS Slow Positron Beam Experiment in Como

In the framework of the cooperation between the AVL-List company in Graz/Austria and the AEgIS group at CERN, a part of the measurements where made at the VEPAS (Variable Energy Positron Annihilation Spectroscopy) positron laboratory in Como/Italy, a member of the AEgIS collaboration. The measurements could be performed with the support of Prof. Rafael Ferragut from the Como group. Two different positron annihilation spectroscopy (PAS) techniques were used: Doppler-broadening spectroscopy and positronium spectroscopy. By means of these methods the non-destructive study of defects and voids in solids is feasible.

The VEPAS positron system is operating since 2010 and is working with a continuous positron beam compared to the pulsed beam of the AEgIS experiment, therefore no positron trap or accumulator are needed in the experimental setup.

2.4.1 ^{22}Na-Source, Tungsten-Moderator and e^+-Transport

A ^{22}Na source with an activity of 15 mCi (555 MBq) is used as a positron emitter. A Tungsten foil with 1 μm thickness is installed in front of the source as a moderator with an efficiency of about 10^{-3} to achieve a monoenergetic positron beam.

From the source the e^+ are emitted with an energy of 1.5 eV and transported via an electrostatic system to the target where a positron current of 10^3 e+/s arrives at the sample on a spot of about 5 mm. The energy of the positron beam is tunable from 0.1 to 20 keV. The beam tube exhibits an L-shape, a deflector is used for bending the beam, see figure 2.12. This ensures the protection of the target area from radiation coming from the source region to suppress the high energy background. The deflector is used to selectively only transport e^+ with the required energy.

For energy tuning and focusing of the beamspot, electrostatic tubular lenses are installed along the beamline at specifically determined potentials.

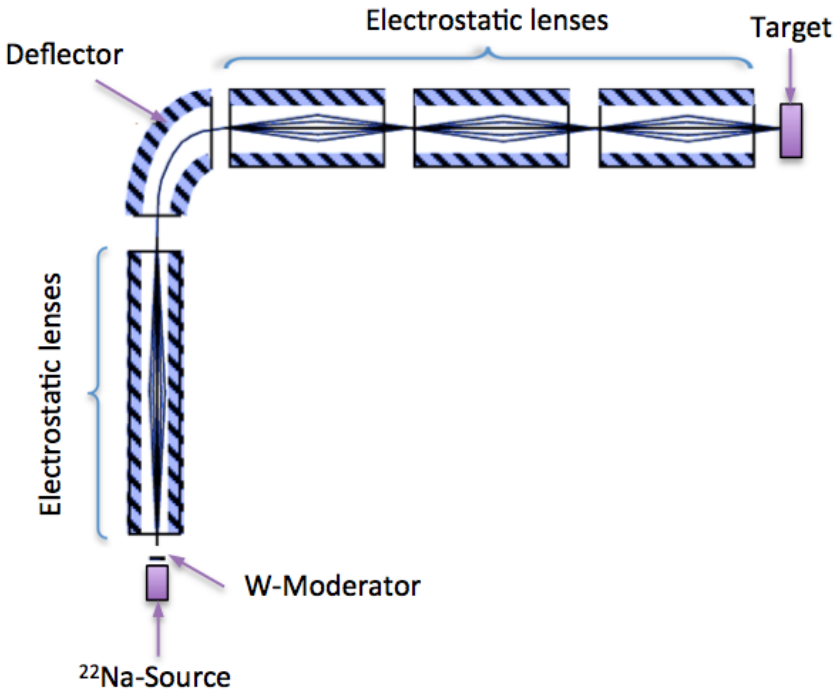

Figure 2.12: Schematic diagram of the experimental set-up of the electrostatic slow-positron beam. The positrons are provided by the ^{22}Na source and pass through the moderator from where they are transported to the target area via electrostatic transport.

The implantation energies can be varied between 0.1 keV and 17 keV. To measure samples at different implantation energies and implantation depths an automated energy scan is implemented. The target region is kept in a high vacuum of about 10^{-9} mbar and offers a variable target temperature of 10 - 1100 K. The slow positron beam has been calibrated for positronium fraction measurements.

2.4.2 Detectors

The system is equipped with Ge detectors for momentum distribution measurements, which can be operated in both single and coincidence mode.

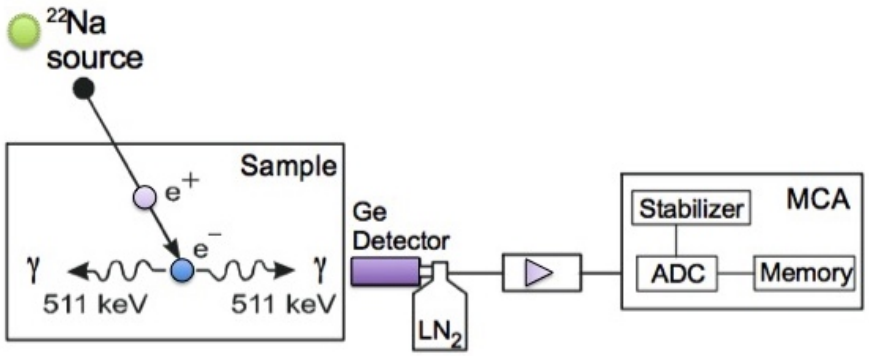

Figure 2.13: Simplified Doppler Broadening experimental setup of the VEPAS slow positron beam. The positron provided by the ^{22}Na source annihilates with an electron inside the sample and 2 γ rays with an energy of 511 keV are emitted. They are detected by 2 HpGe detectors that are cooled with LN_2. The signal is then amplified and digitally stored by an MCA.

The detection system, shown in figure 2.13 measures the energy broadening of the e^-e^+ annihilation radiation as described in chapter 1.6.3. The detectors consist of two high efficiency ultra pure Germanium crystals with an impurity concentration of about 10^{12} atoms/cm^3. They are cooled with liquid Nitrogen (LN_2). The signal induced in the crystals is proportional to the energy of the detected photon. This signal is amplified and digitally stored in a multichannel analyser (MCA). The working principle of this detector is described in chapter 1.5.4.

Background noise can be drastically reduced by using the coincidence mode of the Doppler Broadening method, but was not used in this thesis due to the short time window that was available for the measurements.

2.4.3 Data Analysis

As described in chapter 1.6.3, the Doppler Broadening parameter S was determined. The interval was chosen to $|E - 511|$ keV < 0.85 keV. The S-parameter is sensitive to the low momentum electronic distribution (valence or conduction

band electrons) and to the annihilations of para-Ps annihiliations. The S-parameter is numerically deducted from the energy spectrum by means of a fit program. Measurements were made in dependence of implantation energy. The data analysis was performed with Origin and MATLAB based program (VEPFIT) developed at the VEPAS positron laboratory. [26] The program VEPFIT is based on the numeric solution of the stationary diffusion equation and allows to detect the presence of layers with different characteristics (different structures and materials). In addition, information on the boundaries of different layers and the diffusion length L_+ can be determined.

With the above described apparatus it is also possible to detect ortho-positronium atoms by means of the 3γ annihilation (see chapter 1.6.4). The oPs fraction $F_{3\gamma}$ vs. the energy of the incident positrons can be calculated by means of a semi-linear fitting procedure using VEPFIT, see figure 1.7.

The measuring data taken from both Germanium detectors were imported into the Origin program and subsequently averaged. The error values of the annihilation peak were obtained through the Poisson-distribution.

$$\delta R = \frac{\sqrt{R_{A,B}}}{\sqrt{2}} \tag{2.3}$$

δR... Error for R

$R_{A,B}$... Error of the single detectors A and B

2.5 Positronium Targets

In this chapter the different targets that were tested during this thesis are described in detail. The production method and positronium formation process will be outlined.

2.5.1 Silicon Targets

All samples tested in the AEgIS positron system are made out of silicon and are designed in order to work in reflection mode, emitting positronium back along the direction of the incoming positron beam. These targets are used due to their easy manufacturing process and their well known functionality. The silicon targets were partly produced by the author during the time of this thesis in the group of S. Mariazzi.

To allow for positronium formation, nanochannels are etched into the surface of silicon wafers. This is done through electrochemical etching. The characteristics of the produced e^+/Ps converters depend on the concentration and type of doping of the Silicon wafer (n- or p-type silicon). The doping defines their resistivity and therefore the etching current and the duration of the etching process.
The samples are placed in 75 ml of the etching fluid, made of 47 ml of 48% hydrofluoric acid (HF) and 28 ml of ethanol. An etching current of 10 mA is applied to the solution using two electrodes and is applied for 15 minutes. In the last step the samples are heated to 100 °C, creating a layer of SiO_2 on the surface of the nanochannels. This process is repeated several times to reach the desired size of the nanochannels.

Three different samples with different crystal orientation and type of doping were used. The properties of pores as density, diameter and length depend on the anodization conditions like HF concentration, etching current, silicon type and

resistivity and anodization duration. The production of targets for this thesis aims at maximizing the yield of o-Ps. This depends on the ratio between the volume of the inner silicon pillar and the surface silica layer, and on the pore size. [39] A p-type(100) sample and a p-type(111) sample, each with a resistivity 0.15-0.21 Ω/cm, as well as an n-type(100) sample with a resistivity 0.1-1.0 Ω/cm were used. The p-type(100) target was produced in 2014, while the other two samples were made during the course of this thesis. The p-type(111) target the dimensions of the nanochannels are estimated to 6-8 nm in diameter with a depth of 1-2 μm. The same dimensions are expected for the p-type(100) target, since both p-type samples have the same resistivity. For the p-type(100) target, previously made SEM measurements are available. [39] Since the resistivity of the n-type sample is not very well known, the dimensions of the nanochannels and the etching rate can not be estimated in the same way as for the p-type samples.

The process of positrons entering the sample is shown in Figure 2.14. The target is

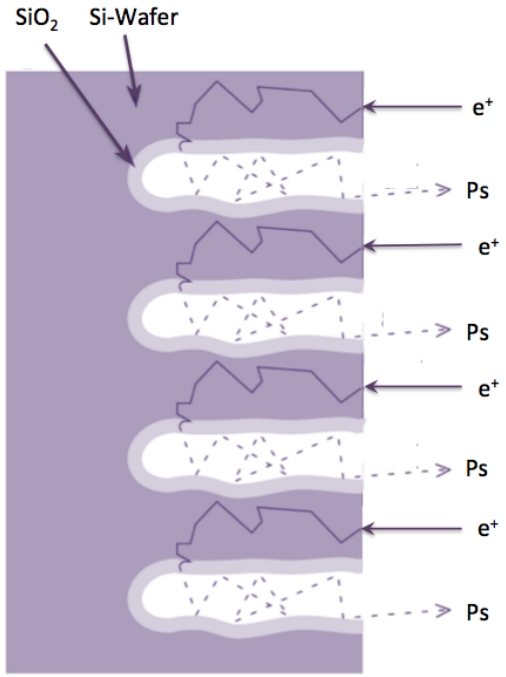

Figure 2.14: Simplified overview of the Ps formation process inside of the nanochanneled Si-targets. Positrons hit the target, thermalize and diffuse into the silicon wafer and form Ps in the SiO_2 layer coating the channels. The Ps atoms then diffuse back to the surface whilst cooling though collisions with the channel walls.

mounted on the aluminum target holder and positioned directly in the line of the beam. The positrons hitting the target thermalize and diffuse through the silicon until they reach the SiO_2 layer inside the nanochannel. The layer serves as an insulator where bulk-Ps is formed and diffuses through the nanochannels towards the surface, where they are emitted from the converter in the direction of the incoming positrons with an energy of several hundreds meV. The Si wafers used are defect-free, moreover no evidence of Ps formation in non-oxidized buried cavities in Si has ever been observed. This makes the SiO_2 covering the channels the only environment for Ps formation. Ps cooling is achieved through collisions of the positronium atoms with the walls of the nanochannels, the energy of the produced positronium depends on the depth of the channels.

2.5.2 Diesel Particulate Filter Samples (AVL)

The two samples provided by the AVL are grids made out of 100% electrodeposited Nickel, 6 μm thick and with vertically oriented channels with a diameter of 7,5 μm approximately and a density of 2000 holes/inch. On the surface of one of the samples there is a carbon layer of less then 1 μm thickness. The capsule holding the target is made from Acetal resin, commonly used for machined plastic parts, see figure 2.15.

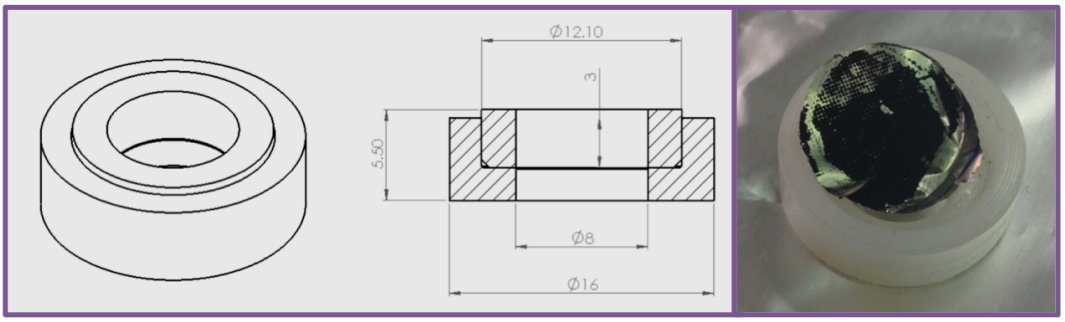

Figure 2.15: On the left: Dimensions of the samples provided by the AVL. On the right: Diesel particulate filter sample with carbon layer that was measured in the Como slow positron beam

The goal for the measurements of these targets was to determine the distribution

of the carbon layer on the surface of the Nickel grid and primarily its penetration into the channels.

Since it is well known that positronium can be emitted from the surface of metallic samples hit by low-energy positrons, the diesel particulate filter substrate made of Nickel is a potential candidate as a e^+/Ps converter. Nickel has a negative positron workfunction of 0.1 eV [40]. For a Ni(100) sample (with carbon contamination on the surface held below < 10 at.%), the positronium work function was determined to Φ_{Ni}= -2,63 $\pm$ 0,26 eV. [41]

3 Results

During the time of this thesis the AEgIS positron system was optimized, updated and fully automated. Some of these optimizations are pointed out in the following section.

In addition to the measurements conducted at the AEgIS experiment at CERN, an investigation of Ps-targets and samples provided by AVL company was performed.

3.1 Comparison of different detectors for SSPALS

To obtain the best possible SSPALS spectra, generated by positron annihilation in the Ps test chamber, different detectors were tested, using an Al target where no Ps is formed and a target with strong Ps formation (p-type(111) Si described in the section 3.3). The measurements were conducted to achieve a comparison of the different detectors available for the AEgIS positron system and to select the most suitable one for Ps detection. All spectra were obtained by averaging over 10 or 20 measurements and normalized to the prompt peak. The spectra were acquired by implanting up to 10^7 positrons in the target. The logarithmic representation accentuates the part of the curve following the peak, which highlights positronium formation.

Firstly, as a comparison, a R11265-100 PMT and a H3378 PMT coupled to a plastic scintillator were tested. The results are shown in figure 3.1.

The e^+ lifetime spectrum obtained with the R11265-100 PMT shows a low level of noise and shows a continuous decrease after the peak. The spectrum recorded

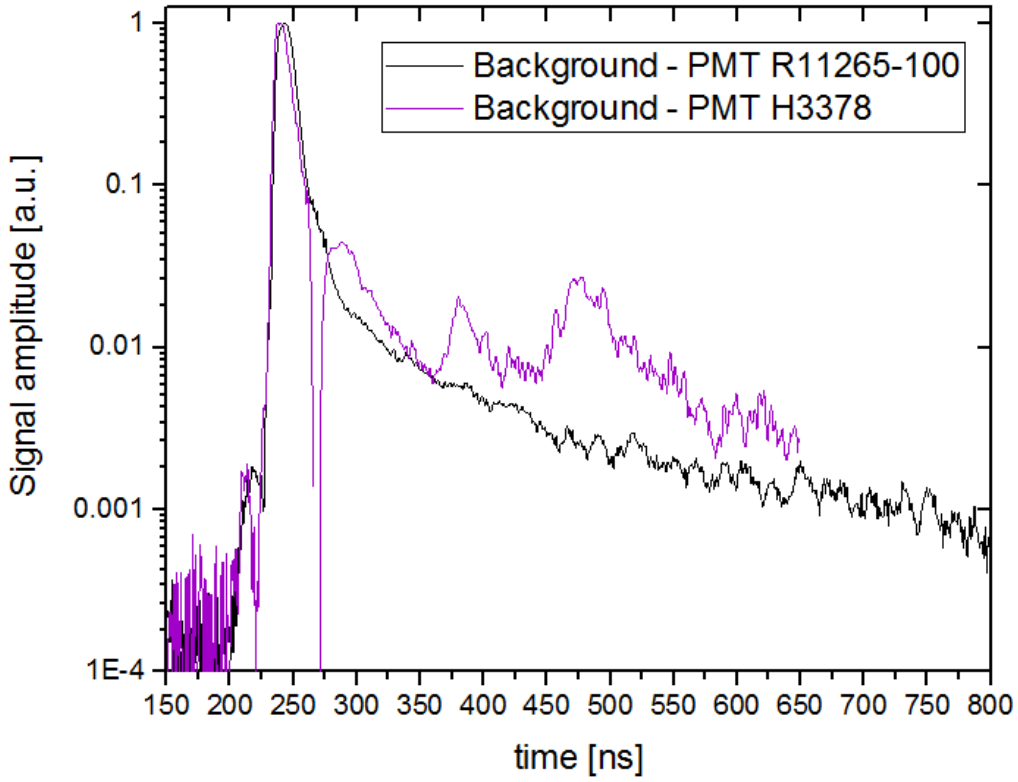

Figure 3.1: Comparison of a a R11265-100 PMT (dark purple curve) and a H3378 PMT (light purple curve) coupled to a plastic scintillator for positron annihilation signals on the aluminium target holder. The curves are an average of 20 measurements and normalized to the prompt peak. The signal of the H3378 PMT is cut off after 650 ns due to the settings on the oscilloscope during these measurements.

using the H3378 PMT shows a much higher noise level after the peak and pronounced irregularities of the falling slope. These irregularities are reproducible and are always at the same position with the same magnitude. Therefore, background noise producing these peaks can be excluded and these irregularities are accredited to an internal property of the PMT.

Due to the result of these measurements, the H3378 PMT was no longer used during this thesis. For all further measurements and the comparison of the photon converters, the R11265-100 PMT was used due to its superior performance.

Furthermore, three different scintillator materials were tested: A plastic scintillator, a PbF_2 Cherenkov radiator and a $PbWO_4$ scintillator were tested and compared,

see figures 3.2, 3.3 and 3.4.

The performance comparison of the converters was solely based on the quality of the produced lifetime spectra, the aim of the comparison was an optimization of the measurements planned to be conducted in the main magnets region.

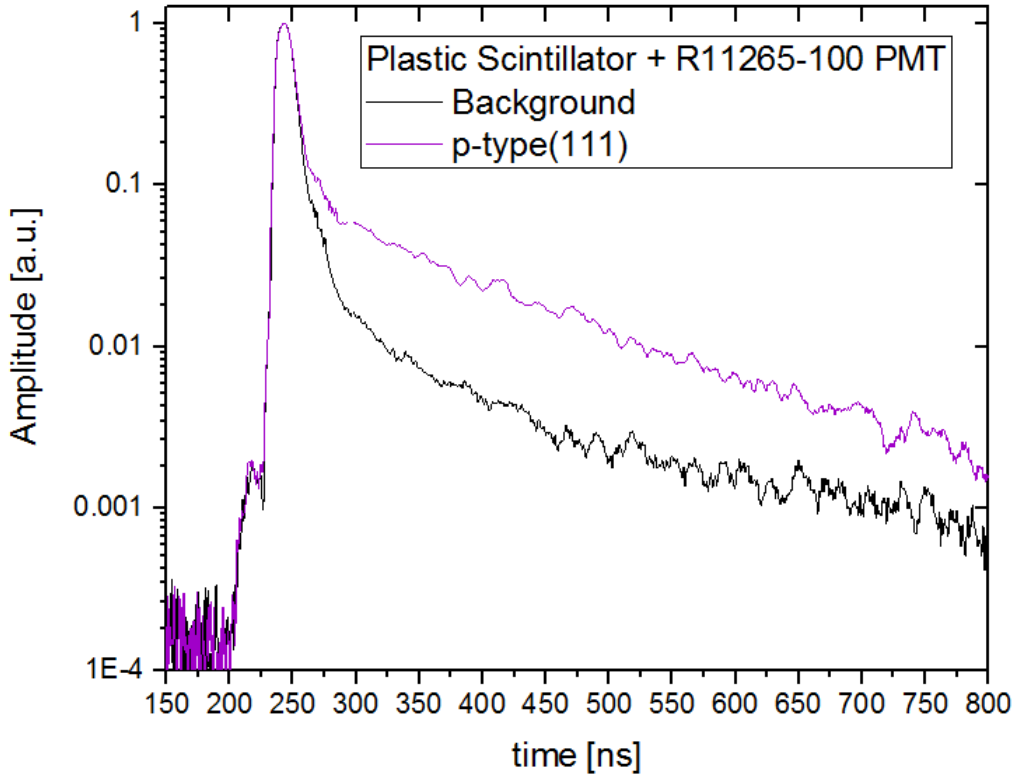

Figure 3.2: SSPALS spectrum measured with a plastic scintillator coupled to a R11265-100 PMT using a p-type(111) target (purple curve) and the aluminium target holder (black curve) for signal without Ps production. The curves are an average of 10 measurements and normalized to the prompt peak.

As shown in figure 3.2, the plastic scintillator coupled to the R11265-100 PMT produces a good signal with low noise levels. However, the annihilation signal without Ps production does not decrease to the level of the background noise during the time span of the measurement. The prompt peak has a width of approximately 9 ns, the background level before the peak has an amplitude of $\sim 2 \times 10^{-4}$. The long tail signifying positronium production is clearly visible.

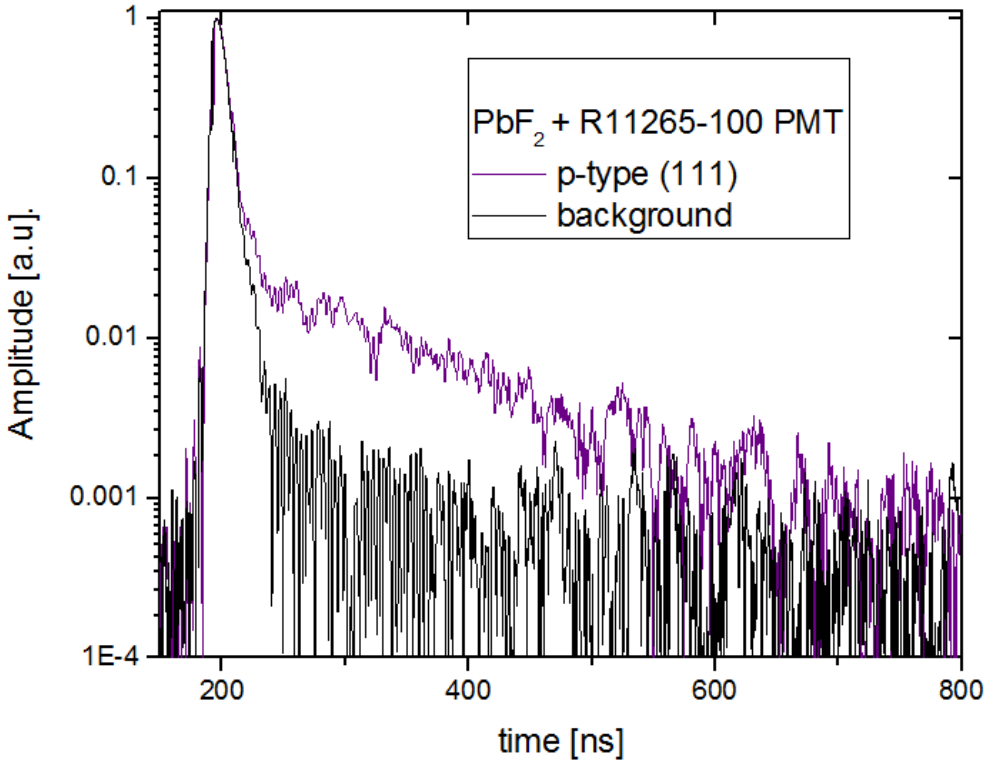

Figure 3.3: SSPALS spectrum measured with a PbF_2 Cherenkov radiator coupled to a R11265-100 PMT using a p-type(111) target (purple curve) and the aluminium target holder (black curve) for signal without Ps production. The curves are an average of 10 measurements and normalized to the prompt peak.

The signal of the PbF_2 Cherenkov scintillator, shown in figure 3.3, is very noisy and the long tail for positronium formation is not as well distinguished as for the plastic scintillator. The signal without Ps production is dropping quite fast to background noise levels. The PbF_2 scintillator shows a high noise level and a very narrow peak with a width of approximately 7 ns.

In figure 3.4 the $PbWO_4$ scintillator has a quite high background noise level with an amplitude of 10^{-3} and peak width of 18 ns. It provides a very low noise signal after the peak and a well distinguished long tail showing positronium production. The signal without Ps formation drops to the background noise level very quickly.

The ideal photon detector for the SSPALS method should have a low noise level, a narrow prompt peak and a fast falling slope in the background spectrum.

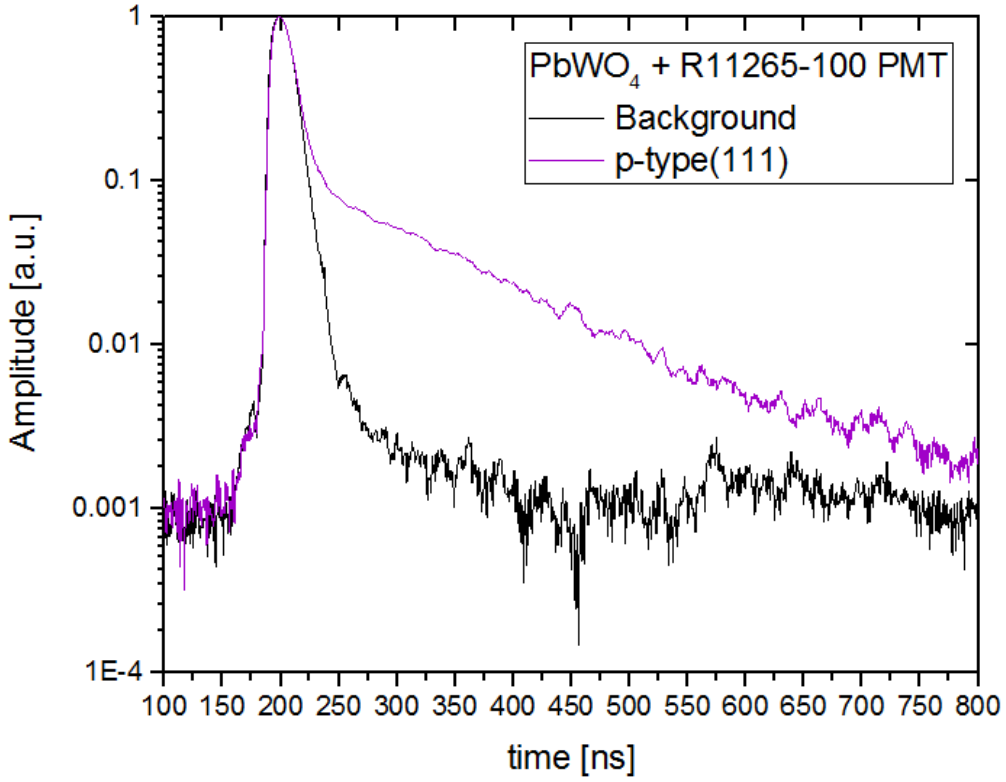

Figure 3.4: SSPALS spectrum measured with a $PbWO_4$ scintillator coupled to a R11265-100 PMT using a p-type(111) target (purple curve) and the aluminium target holder (black curve) for signal without Ps production. The curves are an average of 10 measurements and normalized to the prompt peak

The PbF_2 (figure 3.3) offered the narrowest prompt peak of all tested converters, with a fast falling slope, but a very high noise level, due to its low quantum efficiency, resulting in a low amplitude and making it too noisy for the SSPALS measurements. In the future this could possibly be avoided by installing a voltage amplifier in the present configuration before the data transfer to the oscilloscope and/or by improving the solid angle seen by the crystal.
The plastic scintillator (figure 3.2) showed a delayed falling slope and broadened prompt peak, probably due to the property of after-glow (delay in the fluorescence process) typical for plastic crystals, making it difficult to distinguish positronium formation. A broadening of the prompt peak can also be observed for the $PbWO_4$ (figure 3.4) .

None of the tested detectors are ideal for SSPALS measurements, but the most

suitable detector to investigate positronium formation and compare different e^+/Ps converters, fitting the requirements of the AEgIS positron system best, was decided to be the $PbWO_4$ detector, due to its very low noise signal after the peak, a well distinguished long tail showing positronium production and a fast falling slope to the background signal. The $PbWO_4$ was used for all further measurements of positronium targets and for laser excitation.

3.2 Implementation of a buncher in the AEgIS Positron System

The implementation of a buncher in the positron system was done during the time of this thesis and the results were published in **Nuclear Instruments and Methods in Physics Research Section B**: *Beam Interactions with Materials and Atoms*, in the course of this work, with L. Marx being a co-author. [42]

The buncher was introduced into the positron system to reduce the time spread of the positron pulse supplied from the accumulator. The basic working principle was described in chapter 2.2.5.

The buncher consists of 25 electrodes, forming a parabolic potential up to 10 kV between the first and last electrode, accelerating positrons arriving later (end of cloud) more strongly that the ones arriving early (closer to the Ps test chamber). This reduces the time spread of the bunch. The parabolic function has a variable amplitude and is superimposed to a tunable bias to accelerate the positrons towards the target, see figure 3.5. The combined high voltage pulse has a pulse duration of 30 ns and a rise time of 2-3 ns.

The time shape of the buncher potential was recorded at the entrance of the buncher and is shown in figure 3.6.

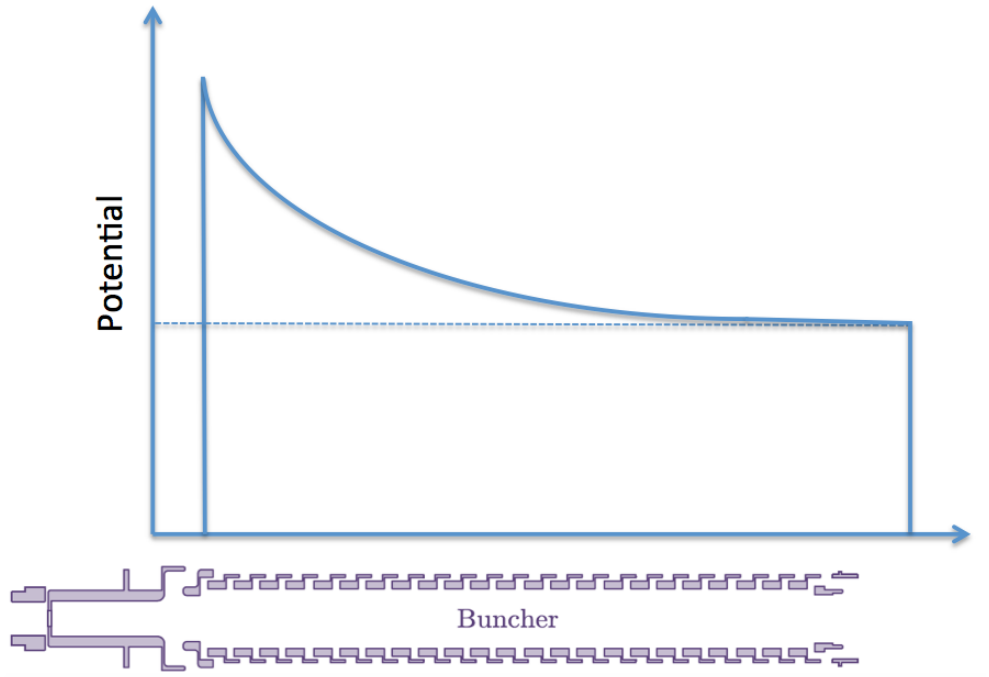

Figure 3.5: Scheme of the parabolic potential superimposed on a high voltage potential of the positron buncher for reduction of the time spread of the positron cloud and e^+ acceleration. In the graph the positrons enter the buncher from the left. When the buncher is turned on with the right timing (i.e. the whole e^+ pulse is inside of the buncher) the positrons entering last are accelerated more strongly than the positrons entering first.

The implementation of the buncher required a lot of different tests and measurements, which were the tasks conducted by the author of this thesis in the group of S. Mariazzi.

The first step was to correctly time the dump from the accumulator to the switch-on of the buncher. It was achieved through a digital delay generator (Stanford Research Systems DG 645). With a length of the buncher of 40 cm and a length of about 20 cm for the positron bunch, the velocity of e^+ is limited to an energy not exceeding 100 eV for optimized compression. Due to the delays from the trigger of the digital delay generator and from the electronics of the buncher and the accumulator, the timing of the buncher switch-on is very important and has to be executed very precisely. An activation too early would lead to a reflection of the positrons on the first electrode of the buncher and a belated activation would result in only a fraction of positrons being accelerated or nor effect at all. To find

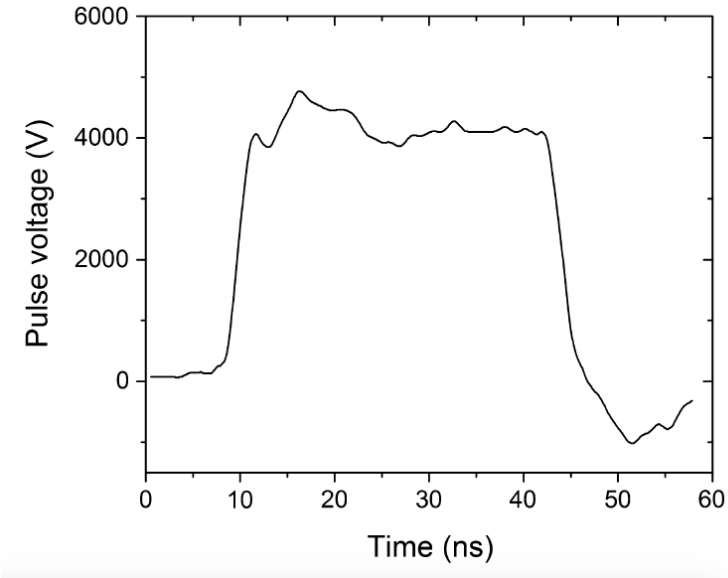

Figure 3.6: Measured shape of the high voltage pulse used for compression of an e^+ pulse in time and space, as a function of time. The signal was acquired at the entrance of the buncher and measured using a Magnelab CT-C1.0 current transformer

the optimum delay time, the signal amplitude of positrons in the main magnets region was measured as a function of the switch-on time, see Figure 3.7.

The peak lies at approximately 20 ns, which signifies the proper delay-time after the positron dump from the accumulator. If the buncher is turned on too early, with a time delay of t< 10 ns the positrons are reflected completely towards the accumulator and no signal can be recorded in the experimental chamber. For a time delay of 10< t <20 ns the e^+ bunch is partly cut off, with a signal amplitude of around 40 mV corresponding to approximately 10^6 positrons hitting the target. For longer delay times the signal amplitude decreases again, due to bad compression. The number of positrons reaching the target does not change but they are distributed over a longer time window, causing a decreased peak amplitude. With a delay of about 20 ns, the signal amplitude is almost three times higher, reaching a value of around 110 mV, corresponding to approximately 10^7 positrons reaching the target.

These results could be confirmed by recording the FWHM of the annihilation signal as a function of the time delay. A broadening of the e^+-lifetime spectrum,

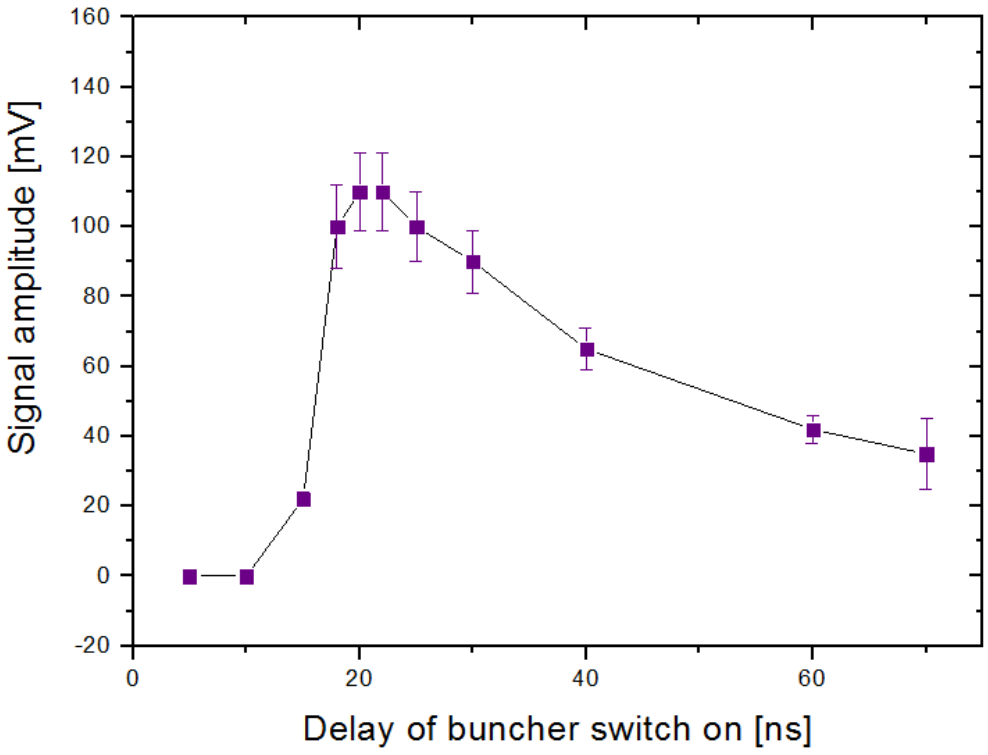

Figure 3.7: Signal amplitude, proportional to the number of positrons annihilating on the aluminium target holder as a function of the delay time of the buncher switch-on after the e^+ pulse has been dumped from the accumulator. The signal was obtained using a PbF_2 Cherenkov radiator coupled to a R11265-100 PMT with 1000 pulses from the accumulator and a positron implantation energy of 3,3 kV. Some error bars are not visible, since they are smaller than the size of the squares signifying the data points.

caused by the widening of the beam pulse was observed as is shown in 3.8.

For optimal bunching a delay time of 18-25 ns is used. For a time delay of less than 18 ns the results are not relevant since only a fraction of positrons or no positrons at all reach the target, which leads to more narrow annihilation peak due to the diminished number of e^+. For a delay time of more than 40 ns the positron bunch is not or only partially compressed, since the e^+ pass through without being influenced by the buncher. For a delay time of $\sim$ 20 ns a minimum FWHM of 7-9 ns is achieved.

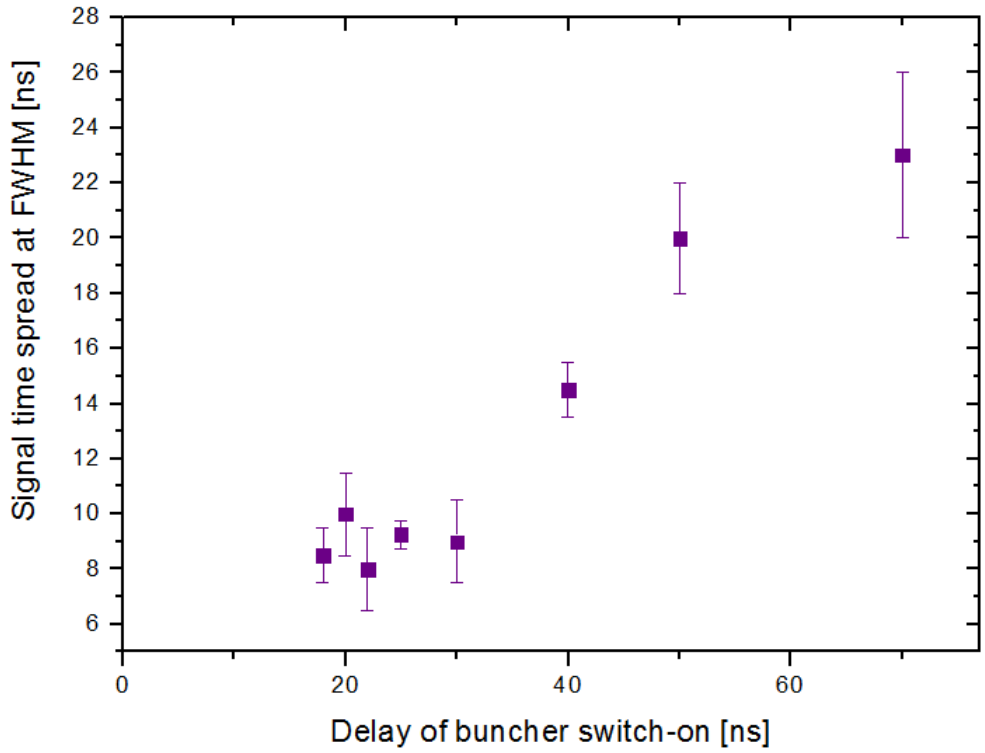

Figure 3.8: FWHM of the e^+-lifetime spectrum in dependence of the delay time of the buncher. Each data point is averaged over 5 measurements, the error bars were calculated through the standard deviation method.

Figure 3.9 demonstrates the effect of beam bunching by means of comparison with a spectrum recorded without bunching. The signal width of $\sim$ 21 ns without buncher could be compressed to $\sim$ 7 ns when the buncher is turned on with the right time delay.

In addition to optimizing the delay time of the buncher, a microchannel plate (MCP) assembly (Hamamatsu F2222–21P25 + Phosphor Screen P46), placed 1 cm behind the target, was used for the characterization of the positron spot size at the target position, see figure 2.9. By removing the sample holder, the positrons could be dumped directly onto the MCP. By means of combining a phosphor screen and a charge-coupled device (CCD) camera, the positron pulse can be imaged and recorded. This image can be seen in figure 3.10.

Figure 3.10 (a) was recorded with electrostatic transport used for guiding e^+ and without a magnetic field in the target region, figure 3.10 (b) shows the

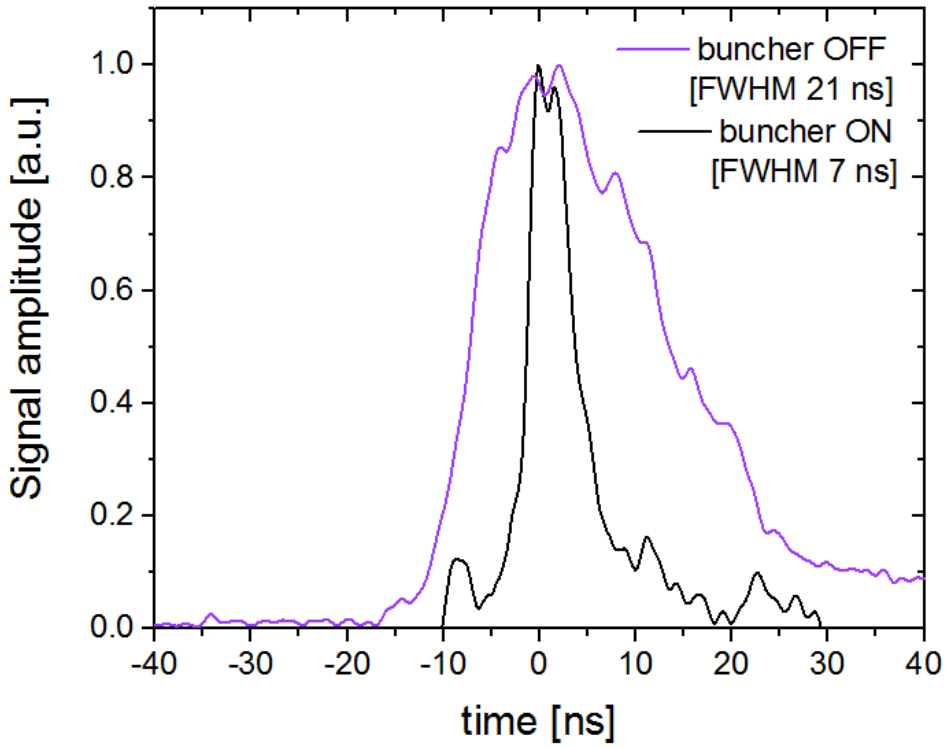

Figure 3.9: Comparison of the FWHM of the positron pulse with the buncher switched on (dark curve, time delay of 20 ns) and with the buncher switched off (light curve).

corresponding intensity distribution with a beam spot diameter of less than 4 mm.

An estimate of the transport efficiency of e^+ along the buncher amounted to $\sim$ 30 % which was obtained by placing a calibrated CsI detector coupled to photodiodes at the entrance and exit of the buncher. The spot recorded in figure 3.10 (a) contains 10^7 annihilation events when 3×10^7 e^+ are dumped from the accumulator.

Measurements of the magnetic field in the target region were obtained with a 3D Hall sensor and showed a field of less than 1.8 Gauss parallel to the beam and less than 0.5 Gauss in the direction perpendicular to the beam. To conduct experiments in a specific magnetic environment, two coils were installed in the target area, able to generate a magnetic field up to 300 Gauss, parallel to the e^+ beam. For a field larger than 150 Gauss, a positive effect on the e^+ extraction from the buncher can be observed, about 40% of positrons dumped from the

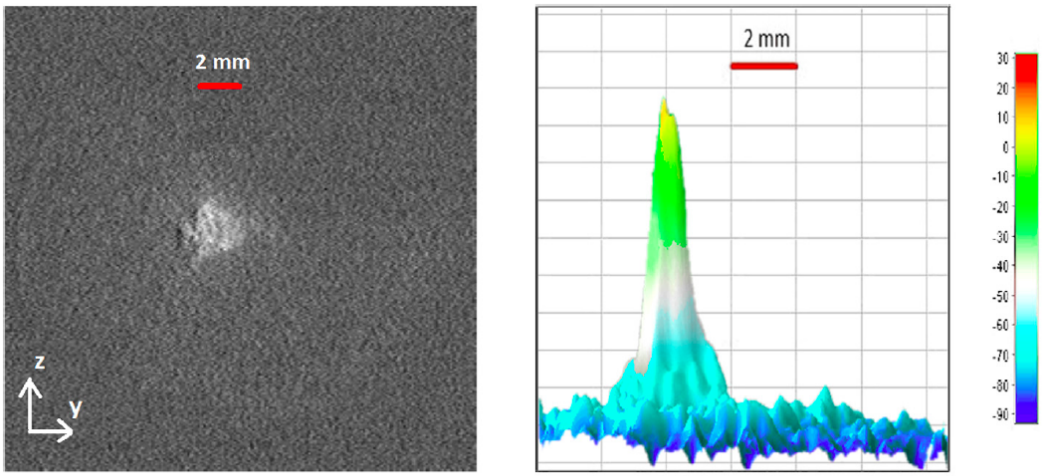

Figure 3.10: Image of the positron beam spot acquired with an MCP assembly and CCD camera, without a magnetic field in the target region and a positron energy of 3.3 keV: (a) shows the radial distribution of e^+ and (b) the corresponding intensity distribution. A beam spot diameter of less than 4 mm was obtained.

accumulator reach the target, which means an improvement of approximately 10%.

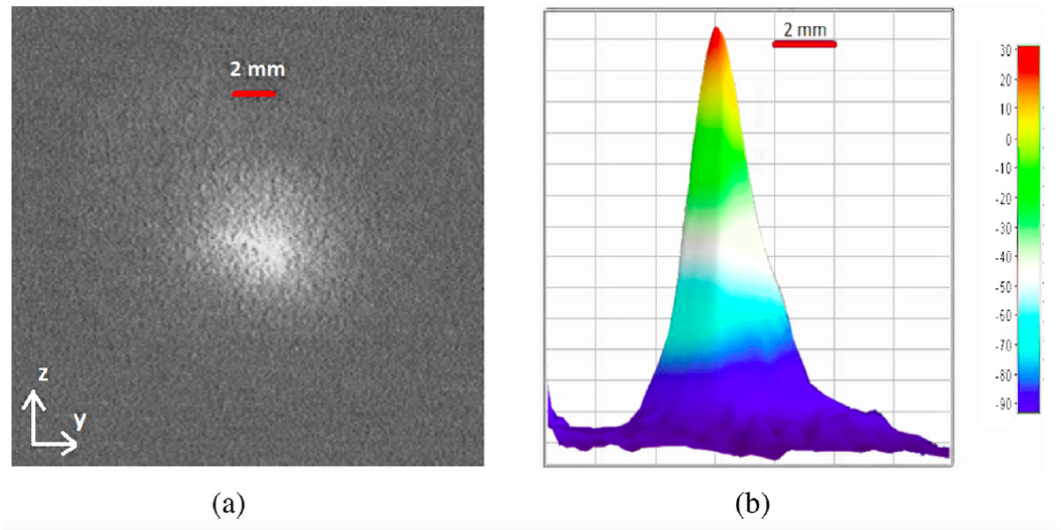

Figure 3.11: Image of the positron beam spot acquired with an MCP assembly and CCD camera, with a magnetic field of 250 Gauss in the target region and a positron energy of 3.3 keV: (a) shows the radial distribution of e^+ and (b) the corresponding intensity distribution. A beam spot diameter of less than 5 mm was obtained.

Figure 3.11 (a) shows the characterization of the positron beam on the MCP with

a 250 Gauss magnetic field in the target area and the corresponding intensity distribution in 3.11 (b), with a beam spot diameter of approximately 5 mm. In this configuration about 1.2×10^7 positrons reach the target when 3×10^7 positrons are dumped from the accumulator. [42]

The largest positron losses occur due to switching between magnetic and electrostatic transport at the entrance of the buncher. This was tested by measuring e^+ annihilation signals at different points of the transfer line.

In summary, an improvement in signal amplitude could be obtained from 40 mV before the implementation of the buncher to 110 mV after the implementation; in addition, a compression in time of the positron bunch from 21 ns to 7 ns could be achieved. A higher transport efficiency of e^+ from the accumulator was recorded for a magnetic field of more than 150 Gauss in the target region.

3.3 Comparison of different Targets for Positronium Production

To find the most suitable positron-positronium converters for the AEgIS experiment and for antihydrogen production in the future, the targets were analysed using scanning electron microscopy(SEM) and first measurements for target suitability were conducted at the slow positron beam in Como. Different silicon based targets where tested in the Ps test chamber of the AEgIS positron system at CERN.

3.3.1 SEM-Measurements of the Positronium Targets

Two nanochanneled silicon Ps-targets of the AEgIS positron group, namely a p-type(111) and n-type(100) sample, were examined at a nanometer scale with a ZEISS scanning electron microscope (SEM) at CERN. The results can be seen

in figure 3.12 and figure 3.13 and are consistent with the results of the SSPALS measurements, see below 3.3.3.

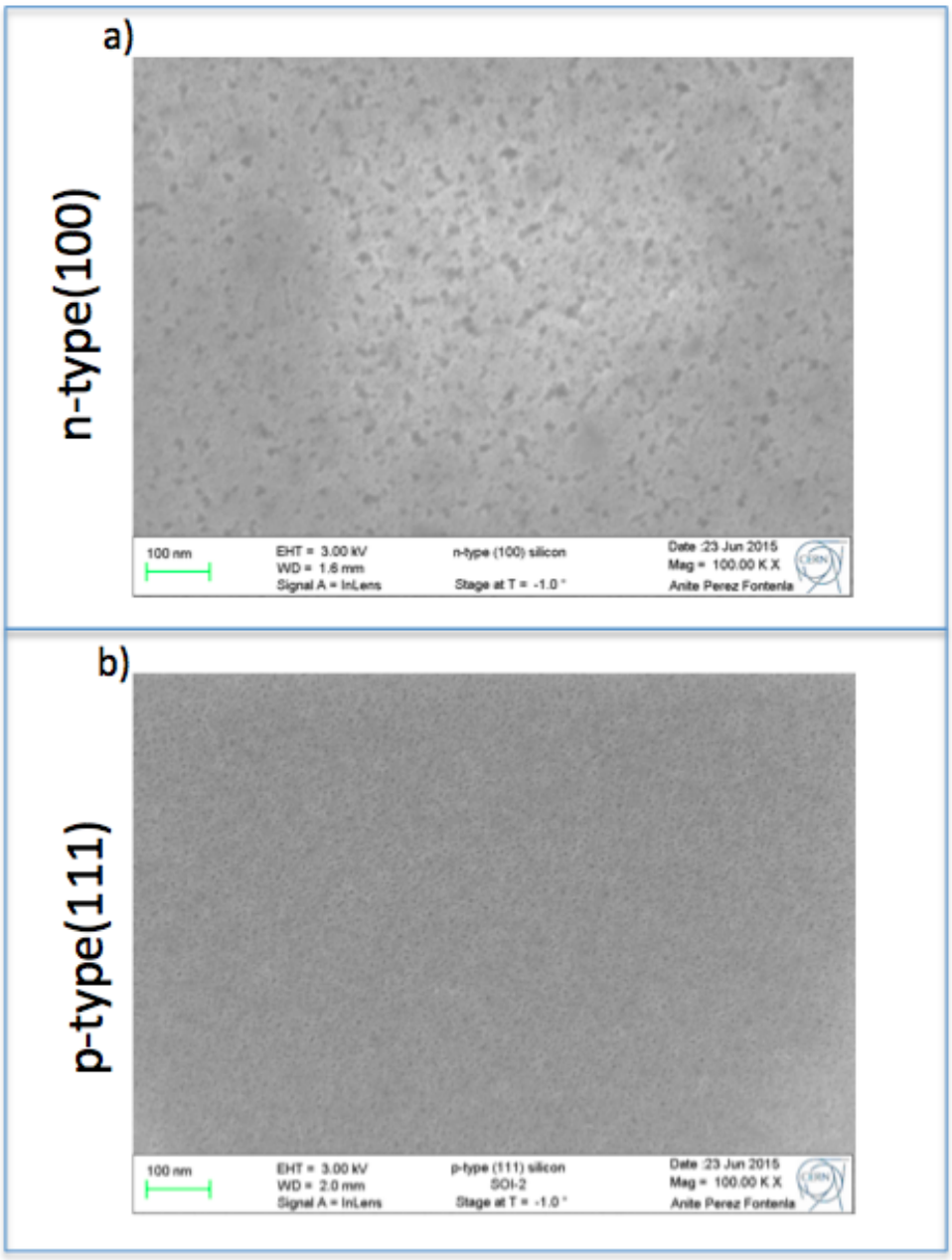

Figure 3.12: Images created with a scanning electron microscope for the n-type(100) sample (a) and the p-type(111) sample (b). The samples were measured perpendicular to the surface with a working distance of 2 mm and a voltage of 2 kV. The lighter areas represent the silicon wafer, the dark patches indicate the nanochannels produced during the etching process. A clear difference in channel size and homogeneity is visible. The p-type(111) sample shows small and regular channels while the n-type(100) sample exhibits a variety of different channel sizes an shapes, with a much lower overall number of channels.

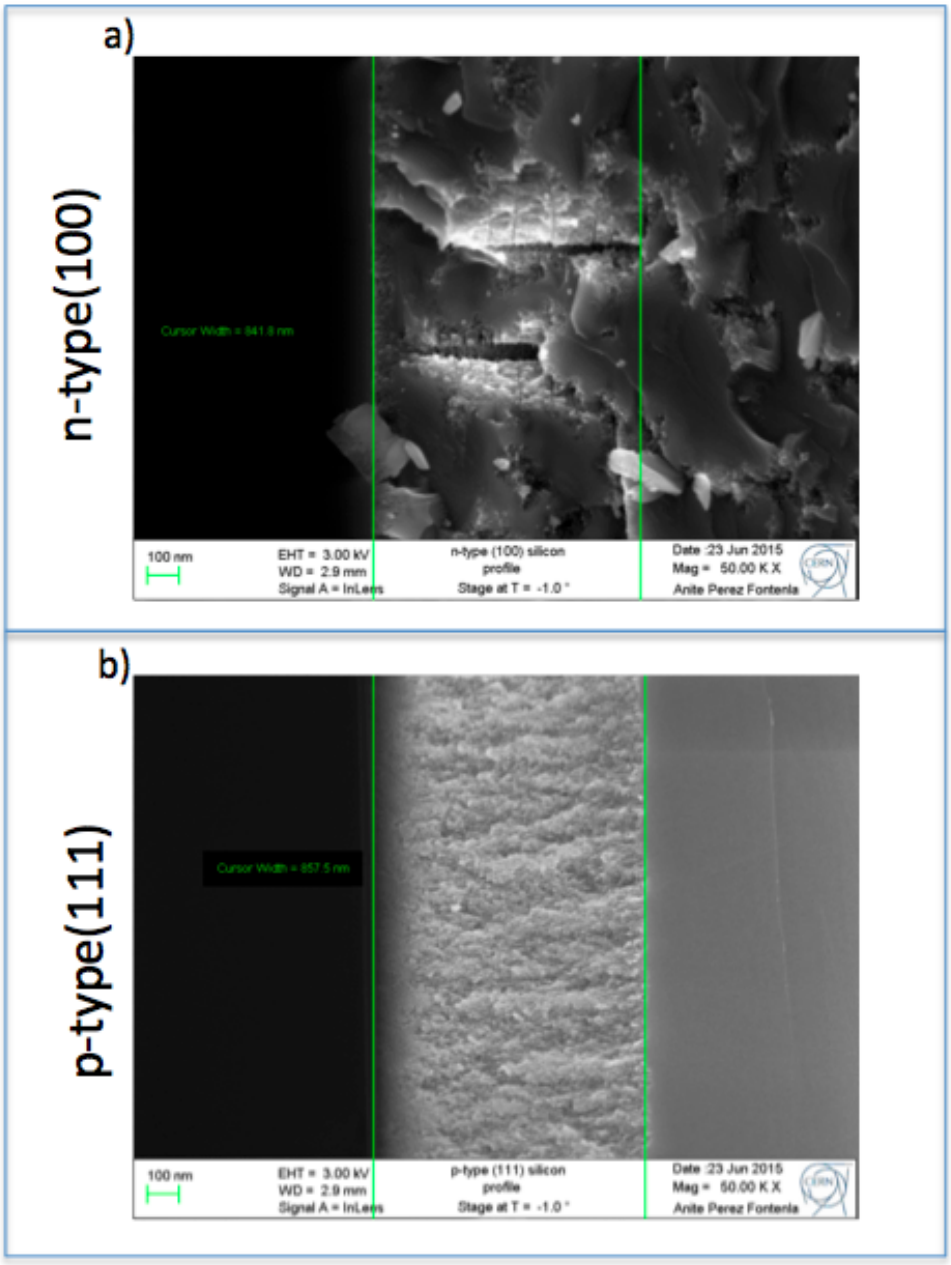

Figure 3.13: Images created with a scanning electron microscope for the n-type(100) sample (a) and the p-type(111) sample (b). The samples were manually broken in half to measure the profile of the sample and the depth of the channels. The measurement was obtained at a working distance of 2.9 mm and a voltage of 3 kV. The p-type(111) sample shows a clear layer effected by the etching process (between the green lines) with a width of about 860 nm, adjoining to the homogeneous silicon wafer on the right hand side of the image. The lighter areas of the image represent the SiO_2 layer. The n-type(100) sample on the other hand, shows no clear boundaries and the visible channels appear very large and irregular.

A clear difference can be the seen between the n-type(100) and p-type(111) samples from both viewpoints. The channels of the n-type sample are irregular,

both in their size and their distribution. The channels of the p-type sample are significantly smaller, constant in size and regularly distributed. The images in side-face view, have to be interpreted with care, since the breaking process is not well controlled. In contrast to the n-type sample the p-type sample shows a clear SiO_2 layer in the side-face view and channels reaching approximately 860 nm into the wafer, which yields the base for the high positronium yield for this sample,, see 3.3.2. Only few and irregular channels can be seen for the n-type sample in figure 3.13 a) with no clear SiO_2 (lighter areas), which is in accordance with the very low positronium yield that was measured for this sample. This is probably due to the etching process, that might not be as well suited for the resistivity of the n-type samples, see chapter 2.5.1.

3.3.2 Measurements at the VEPAS Laboratory/Como

In the framework of the cooperation between the AVL in Graz/Austria and the AEgIS group at CERN, a part of the measurements for the characterization of samples for Ps production were made at the VEPAS (Variable Energy Positron Annihilation Spectroscopy) positron laboratory in Como/Italy. Two different positron annihilation spectroscopy (PAS) techniques were used: Doppler-broadening spectroscopy and positronium spectroscopy. The measurements should serve as a test for the suitability of the investigation method.

The measurements were obtained in two runs of 1000 s per implantation energy varying between 0,1 and 17 keV for each sample. The Data-Analysis tool used to process the obtained data was the Origin and Matlab based program VEPFIT and described in the previous chapter 1.6.3. Measurements of the Doppler Broadening parameter S and the positronium fraction $F_{3\gamma}$ vs. the energy of the incident positrons were analysed by means of a semi-linear fitting procedure. A background measurement was obtained for 70000 s with 0,03 counts/s compared to 5 counts/s for the positron annihilation signal. This results in a peak to background ratio of P/B=170.

Positronium spectroscopy

The results of the positronium spectroscopy measurements can be seen in figure 3.14. Two reference spectra were used, namely an Aerogel 85 sample (density 85 mg/cm^3) and a monoUTHClAl sample consisting of a porous silicon material with a Calcium phosphate layer and thin film of aluminum (70 nm). Two nanochanneled silicon Ps-targets of the AEgIS positron system were measured (p-type(111) and n-type(100)) in addition to the two diesel particulate filter samples provided by AVL (figure 3.14).

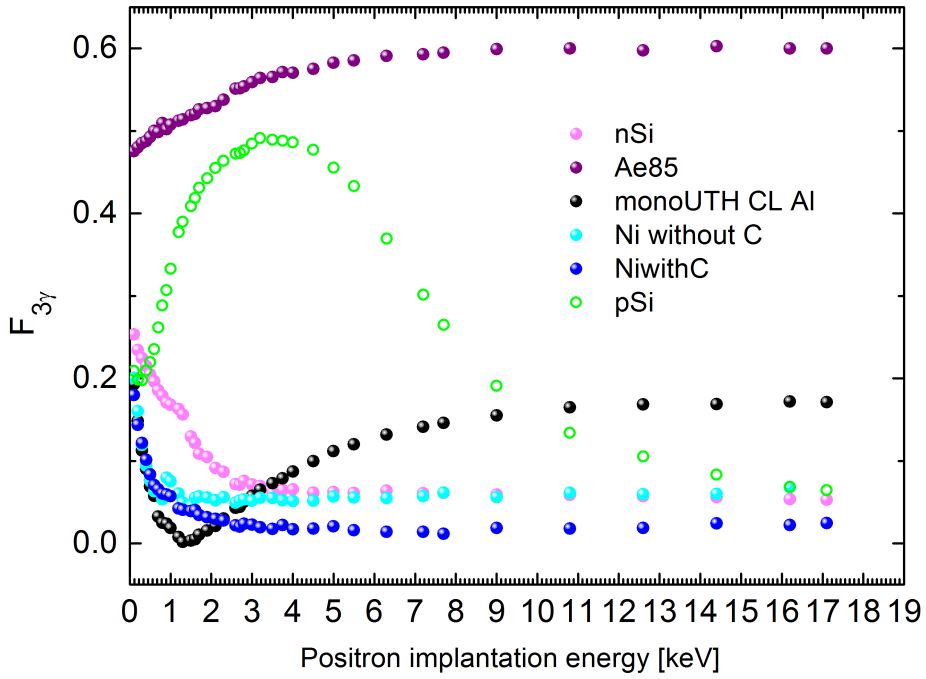

Figure 3.14: Measurements of the positronium fraction $F_{3\gamma}$ over the positron implantation energy (0,1-17 keV) obtained with the positronium spectroscopy method for 6 different samples. The Aerogel 85 sample (dark purple) and the monoUTHClAl sample (black) represent the reference samples to calculate the specific Ps fractions. The n-type Silicon (pink) and p-type silicon (green) samples represent the measurements of the nanochanneled Ps-targets of the AEgIS positron system. The curves of the nickel targets with (dark blue) and without carbon (light blue), show the measurements of the investigated diesel particulate filter samples provided by the AVL.

The Positronium fraction $F_{3\gamma}$ was calculated using the following equation:

$$F_{3\gamma} = [1 + \beta \times (\frac{R_1 - R}{R - R_0})]^{-1} \tag{3.1}$$

- $F_{3\gamma}$ ... Ps formation fraction
- β ... Corresponds to a globally used parameter obtained by the ratio of the peak areas for 0% (P_0) and 100% (P_1) positronium production. $\beta = \frac{p_1}{p_0} = 0.44$ is obtained after background subtraction. It is not as strongly dependent on the apparatus, environment and material as R_0 or R_1 and can therefore be used globally.
- R ... Measured R-parameter value for the examined sample at a certain implantation energy
- R_0 ... R-parameter which corresponds to the value for 0% Ps production. R_0 ... is calculated from the lowest point of a reference spectrum of a porous silicon material with a Calcium phosphate layer and thin film of aluminium (70 nm)) (see figure 3.14) which provides a very low Ps yield. Due to physical properties, the R_0-value does not precisely represent 0 % of positronium production but a very low value between $1\% - 3\%$, which introduces a small error. R_0 depends on the density of the detector material.
- R_1 ... R-parameter value corresponding to 100% Ps production, can in reverse be calculated from the above equation by inserting R_0 from above and $R_{60\%}$ which is obtained from the average of the five highest values of the reference spectrum from an Aerogel 85 target (density ρ= 85 mg/cm^3), which has a known $Ps_{3\gamma}$ annihilation rate of approximately 60%. R_1 would correspond to the measurement of a Germanium target at 1000 K for 100% Ps yield [43] and amounts to R_1= 2,4805 for the measurements discussed here.

A high positronium yield was measured for the p-type(111) sample with a peak at around 3,5 keV, in comparison to a very low Ps production rate for the n-type(100) sample. This is in accordance to the results obtained at the AEgIS positron system and the SEM-measurements described above.

As expected, the pure nickel sample without carbon is very uniform, a very low $F_{3\gamma}$ rate can be seen. The measurement of the nickel sample with carbon layer shows the same uniform curve but with a consistently lower $F_{3\gamma}$ value. For a pure nickel sample, no significant Ps production is expected. The obtained signal could stem from Ps production on the sample surface that is suppressed by the carbon layer for the second sample. To confirm this assumption and find out more about the samples, further measurements are necessary, including higher statistics and the modification of the sample through the removal of the carbon layer. This would be of interest due to how little is known about the deposition process of the nickel substrate and the application of the carbon layer.

For the p-type(111) silicon sample a value $F_{3\gamma} \approx 50\%$ is calculated from the peak value at around 3,5 keV. At the same energy a positronium fraction of only $F_{3\gamma} \approx 5\%$ was calculated for the n-type(100) sample, which is supported by the results obtained using scanning electron microscopy in chapter 3.3.1.

The goal of the measurements of different targets, was to test the suitability of the different sampleswith respect to e^+/Ps conversion for the production of positronium for the AEgIS experiment. This leads to the following conclusion:

1. High Ps formation could be observed in the p-type(111) sample.
2. Low Ps formation was evidenced in the n-type(100) sample.
3. No Ps formation was observed in the diesel particulate filter samples.
4. Further investigations are needed to fully characterize the last set of samples.

Doppler Broadening Spectroscopy and Defect Depth Profiling of Diesel particulate filter samples

For numerical analysis of the defect depth profiles, pre-information about the sample and the positron implantation profile is needed. The profile is obtained from Monte-Carlo simulations and from experimental results of Doppler-Broadening spectroscopy by means of the VEPFIT program (see chapter 2).

For the diesel particulate filter samples the density of the nickel substrate was calculated from the known density of nickel ρ = 8,908 g/cm^3 at 20°C. Taking into account the density reduction due to the open channels, with the known dimensions of the open channels in the substrate (7.5 μm channels with 2000 holes/inch [1]) the density of the particulate filter sample could be calculated. A density of ρ= 6,468 g/cm^3 was obtained, which is about 72.6% of the density of pure nickel.

The diffusion length for the pure nickel sample was obtained through VEPFIT: $\bar{d}$=170 nm, for an S-parameter of S = 0.4748 and an implantation energy of 8 keV (figure 3.14). The carbon layer depends on the production method, it is made up of amorphous carbon (information provided by the AVL) which has a density of ρ = 1,8-2,1 g/cm^3. Therefore a value of ρ = 1,95 g/cm^3 was used for the calculations of the depth profile. For modelling, a trilayer structure is assumed, consisting of a pure carbon layer, a potential interface and the porous nickel layer, which can be considered as basically infinite due to its thickness of 6 μm, see figure 3.15.

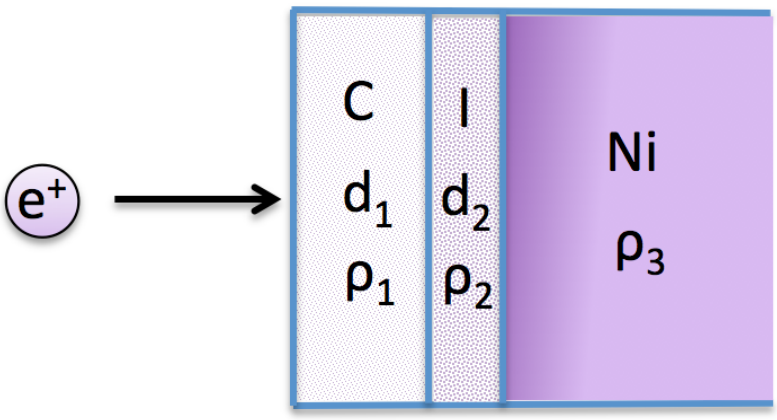

Figure 3.15: Composition of the Ni sample (Ni, density ρ_3), with Carbon layer (C, density ρ_1, thickness d_1). The best fit was obtained by including an thin interface (I, density $\rho_1 2$, thickness d_2).

The mean implantation depth profile provides thickness estimations of the different layers with each implantation energy corresponding to a certain implantation

[1] Information provided by AVL

depth of positrons (8 keV corresponds to about 500 nm). Another assumption had to be made about the density of the potential interface which had to lie in the range of ρ = 1,95-6,5 g/cm^3, i.e., between the values of the nickel substrate and the carbon layer. A value $\rho \approx$ 4,2 g/cm^3 was chosen.

The measured S-parameters for both samples obtained from the measurements through VEPFIT can be seen in figure 3.16.

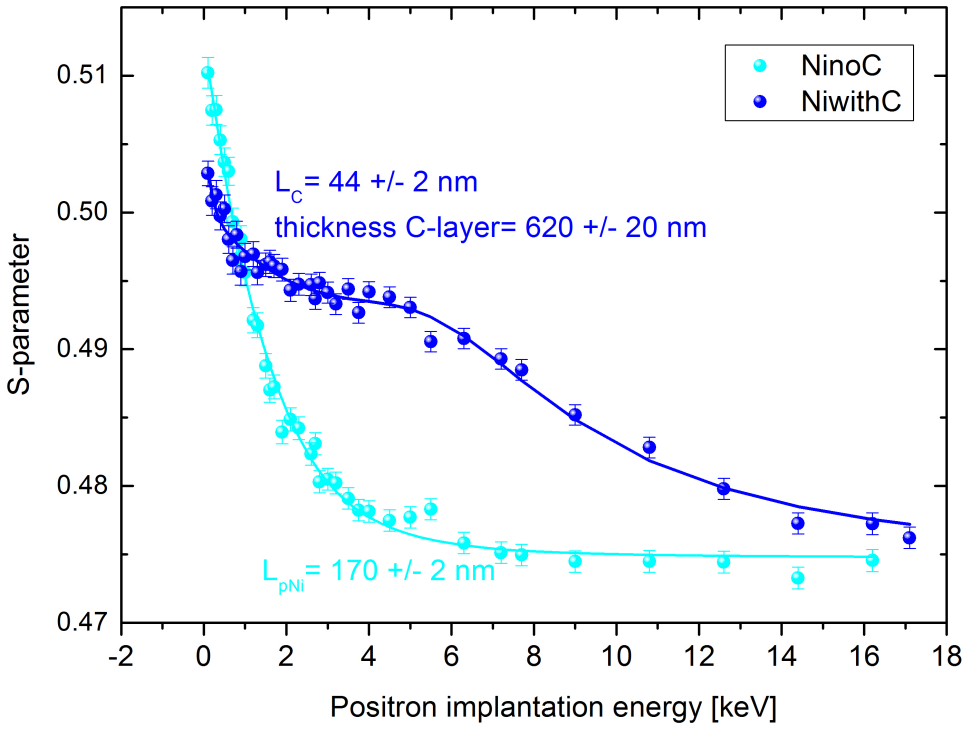

Figure 3.16: S-parameters over the positron implantation energy (0.1-17 keV) obtained through Doppler-Broadening spectroscopy of a nickel sample with (blue curve) and without (turquoise curve) carbon layer with the corresponding fits calculated with VEPFIT, assuming the existence of three different layers. The fit was chosen as the most suitable fit through a Chi-squared test.

For the pure nickel sample the S-parameter continually decreases in the direction of the bulk showing a clear distinction compared to the sample with the added carbon layer. With a third layer being included, the model of the defect depth profile is closest to the experimental reality, but it is not a proof of the existence of the interface, since the interface is not clearly visible, see figure 3.16. The interface

becomes notable in the analysis through the step in the fit of the depth profile. The existence of the step is not clear in the context of statistics. This suggests an interface of a width no wider than 2 nm. A Chi-squared test was used to compare the experimental results with the model values to determine the goodness of the fit. It showed that the inclusion of an interface provided the better fit.
A mean diffusion length of L_C = 44±2 nm was estimated, which suggests a carbon layer containing few pores only. This is symptomatic of a film of good quality and little defects. The thickness of the carbon film was calculated to d_C = 620±20 nm.
Without numerical constraints interface of about d_I = 10 nm was calculated, which is probably overestimated, since this would correspond to a significant layer thickness of about 100 atoms. Since interface is not clearly visible in the measurements, the thickness of the interface was fixed to d_I = 2 nm in the VEPFIT program yielding a mean diffusion length of L_I = 0,04 nm. This represents a diffusion length very close to zero and indicates that the interface contains a high amount of e^+-trapping centres.
For an interface thickness of d_I = 4-5 nm, a diffusion length of L_I = 40 nm was obtained.

The parameters obtained for the pure Ni were used as fixed parameters for the Ni-layer when analysing the C-coated sample. This assumption however, requires that the C-layer does not influence the Ni-substrate, which is not known.
Different densities for the interface were tested, since this density is completely unknown:
ρ = 2,1 g/cm^3 (assuming that the density of carbon is higher) which led to no change in the model.
ρ = 5,5 g/cm^3 which led to a small change in the diffusion length from L_I = 44 nm to L_I = 47 nm.
ρ = 1,6 g/cm^3 (interface density even lower than that of carbon) yields a diffusion length of L_I = 46 nm. These analyses show that the mean diffusion length slightly decreases with reducing the interface density.

It becomes evident that more information about the samples is required in order to make more accurate fits and to perform further investigations.

3.3.3 Measurements at the AEgIS Experiment (CERN)

The measurements were made using the $PbWO_4$ detector coupled to the Hamamatsu R11265-100 PMT, due its superior suitability proven in chapter 3.1. The measurements were done by single shot positronium annihilation lifetime spectroscopy (SSPALS). Three different porous Si samples were tested, made from p-type(111), p-type(100) and n-type(100) Si. The spectra are shown in figure 3.17. Each curve is an average of 10 measurements, the curves have been normalized to the prompt peak. As a reference for the assessment of the background a e^+ lifetime spectrum was measured using an Al sample holder which exhibits no Ps formation.

The rapid decrease of the time signal quite similar to that of a reference sample, indicates that there is no significant Ps formation and annihilation in the porous sample made from n-type Si. The curves of the p-type samples show a considerably higher signal and slower decrease after the e^+ annihilation peak and reach the background noise level after approximately 400 ns. This long tail can be attributed to o-Ps formation, with a lifetime of $\sim$ 142 ns in vacuum. The p-type(111) sample shows a slightly higher signal compared to the p-type(100) sample, which suggests a better positronium production rate. For this reason this sample was used for all later experiments including laser excitation of the created Ps atoms.

The lifetime of the created Ps atoms could extracted from the spectra by fitting them with an exponential decay function, see equation 3.2.

$$N(t) = N_0 e^{\frac{-t}{\tau_{Ps}}} + A \tag{3.2}$$

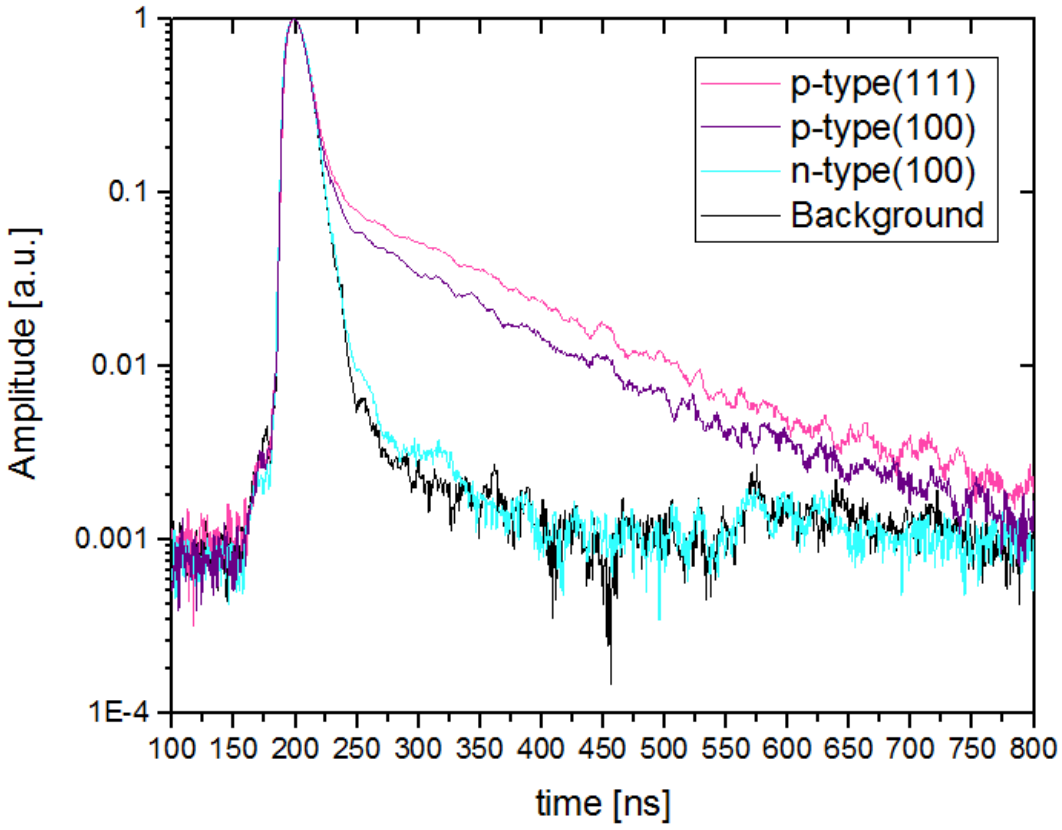

Figure 3.17: SSPALS spectra measured with a $PbWO_4$ scintillator coupled to a R11265-100 PMT comparing nanochanneled silicon targets: A p-type(111) (purple curve), a p-type(100) (pink curve) and a n-type(100) (blue curve) target. For background measurements (black curve) the aluminum target holder was used. The curves are an average of 10 measurements and normalized to the prompt peak.

t... Time passed since start of Ps formation

N(t)... Number of Ps atoms at the time t

N_0 ... Initial number of Ps atoms

τ_{Ps} ... Lifetime of Ps atoms

A ... Constant Term

The characteristic lifetime τ_{PS} denotes the time constant after which the number of positronium atoms has decreased to $\frac{1}{e}$. For the lifetime measurements the background measurement was substracted from the SSPALS spectra and fitted with the exponential decay from equation 3.2. A lifetime of $\tau_{PS} = 142.8 \pm 1$(stat) ns was obtained for the p-type(111) sample by fitting one of the spectra, see figure 3.18. A lifetime of $\tau_{PS} = 111 \pm 1$(stat) ns was obtained for the p-type(100)

sample.

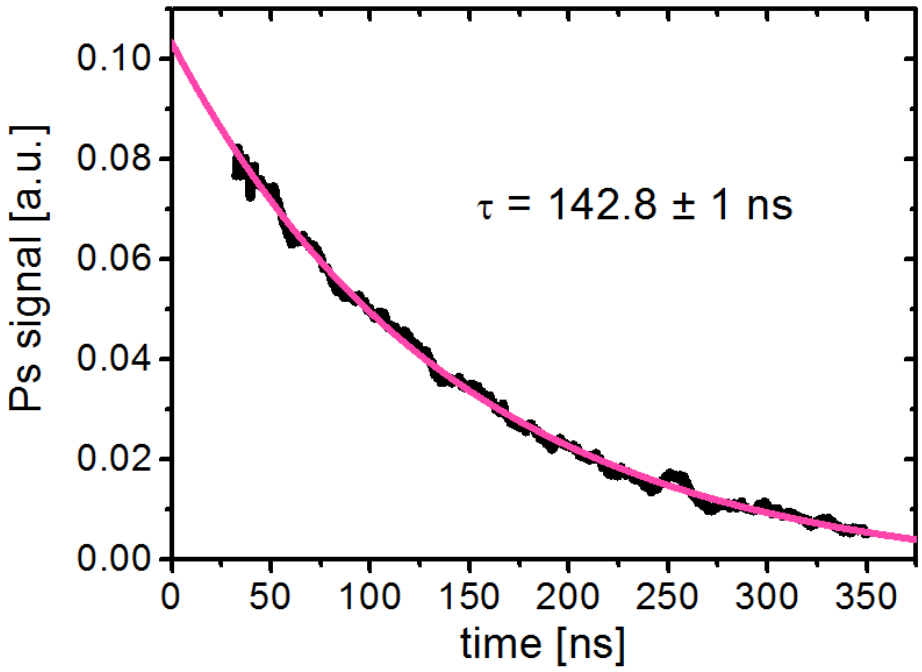

Figure 3.18: Estimated lifetime of the p-type(111) sample, by fitting the SSPALS spectrum with an exponential distribution describing the positronium decay in the 50-350 ns region after the annihilation peak. The background in substracted from the positronium formation measurement. A positronium lifetime of approximately 142 ns was obtained for the p-type(111) sample.

No conclusions about the total Ps fraction can be drawn from the intensity of the spectra, since no reference condition with a Ps fraction of 100% is available. Therefore only a relative comparison of intensities is possible. The larger Ps-fraction obtained for the p-type(111) sample, may arise from the direction of the channels inside the sample. Due to an angle of around 45° the channels of the p-type(111) sample are probably more interconnected than in the p-type(100) sample with 90° channels in reference to the surface [44], therefore the positrons can reach the SiO_2 more easily to form Ps and then leave the sample through the channels. This could also explain the longer lifetime for Ps atoms in the p-type(111) sample, which with 142 ns is equal to the vacuum lifetime. The results of the n-type sample are probably based on an unsuitable etching process, since no formed channels could be seen in the SEM images, see chapter 3.3.1.

4 Evaluation and Outlook

The principle goal of this thesis was the optimization of the AEgIS positron system, to supply Rydberg excited Ps^* atoms for the production of antihydrogen and subsequently for the measurement of the earth's gravitational acceleration on these antimatter atoms.

- Comparison of different detectors:
  To optimize the obtained SSPALS signal, a R11265-100 PMT and a H3378 PMT coupled to a plastic scintillator were compared. The R11265-100 PMT was chosen for all further measurements, because the corresponding SSPALS spectrum exhibits a low level of noise and a continuous curve with a stable descending flank of the time spectrum.
  As photon converter, a plastic scintillator, a PbF_2 Cherenkov radiator and a $PbWO_4$ scintillator were tested and compared. The most suitable converter, fitting the requirements of the AEgIS positron system best, was decided to be the $PbWO_4$ detector, due to its very low noise signal after the peak, a well distinguished long tail showing positronium production and a fast falling slope to the background signal. The $PbWO_4$ was used for all further measurements of positronium targets and for laser excitation.
- Implementation of a Buncher in the positron system:
  A signal width of $\sim$ 21 ns was measured without using the buncher, which was compressed to $\sim$ 7 ns when the buncher was turned on with the right time delay. This results in a positron cloud with a signal time spread much smaller then the lifetime of positronium, making it easier to detect Ps formation and making possible experiments of Ps spectroscopy using SSPALS. A change in signal amplitude was measured from 40 mV before the implementation of the buncher to 110 mV after the implementation. This

optimization is due to the compression of the beam and a higher number of positrons in the area of the prompt peak.

Part of the measurements have been performed at the VEPAS laboratory in Como, using a slow positron beam to investigate two silicon based e^+/Ps converters with nanochannels namely a p-type(111) sample and an n-type(100) positron/positronium converter, as well as the diesel particulate filter samples provided by the AVL company to find the most suitable target for Ps production.

- Silicon based samples:
  A high positronium yield was measured for the p-type(111) sample with a peak at an implantation energy of around 3,5 keV, in comparison to a very low Ps production rate for the n-type(100) sample. For the Ps fraction of the p-type(111) silicon sample, a $F_{3\gamma}$ of 50% is obtained from the peak value at around 3,5 keV. At the same energy a positronium fraction of only $F_{3\gamma} \approx 5\%$ was calculated for the n-type(100) sample.
- Diesel particulate filter samples:
  Positronium Spectroscopy:
  The pure nickel sample without carbon is very uniform, a very low $F_{3\gamma}$ rate can be seen. The measurement of the nickel sample with carbon layer shows the same uniform curve but with a consistently lower $F_{3\gamma}$ value.
  Doppler Broadening Spectroscopy:
  The best fit for the obtained S(E) could be made with the assumption of an interface between the nickel substrate and the carbon layer.
  A mean e^+ diffusion length in the carbon layer of L_C=44$\pm$2 nm was measured, which suggested a carbon film of good quality and little defects. The thickness of the carbon film was calculated to d_C=620$\pm$20 nm.
  To make more accurate predications, additional information about the composition of the sample and the deposition method of the carbon layer is needed.

Based on the results of the measurements mentioned above two silicon based p-type targets and one n-type target were investigated in the Ps test chamber of the AEgIS positron system.

- Comparison of Positron/Positronium converters:
  In a relative comparison of three different Si-based targets with SiO_2 coated nanochannels and with different channel orientations (p-type(111), p-type(100) and n-type(100)) the p-type(111) sample was found to provide the highest o-Ps fraction with the highest Ps lifetime of approximately 142 ns and was used for all further measurements. Also from the results obtained at the VEPAS positron system, the p-type(111) Si was identified as the best e^+ converter.

4.1 Future Work

For the future, further optimization and modification of the Ps system will be necessary to achieve a more stable positron beam and a higher number of positrons in the Ps test chamber.
A new ^{22}Na will be installed in the near future, which will help to raise the number of positrons in the experimental chamber. A complete μ-metal shielding of the positron system has been installed in the meanwhile in order to protect the apparatus from magnetic fields from the AEgIS central region and other experiments in the AD hall.
Colder positronium will be needed to form cold antihydrogen for the gravity measurements. Therefore different techniques for positronium cooling are planned including a higher implantation energy of e^+ together with a larger implantation depth, the use of different targets and the installation of a cryostat, planned in the area of the Ps test chamber. Laser excitation of the produced Ps atoms is currently in progress; it was not discussed in this thesis but it uses the progresses achieved here. Additional measurements for Ps laser excitation via n=3 to Rydberg levels

were proposed for the near future and have partly already been performed during the completion of this work. For antihydrogen production, a e^+/Ps converter in transmission mode will be developed and tested in the Ps test chamber, which is planned to be included in the AEgIS central region during the next years.

For the cooperation between the AEgIS collaboration at CERN and the AVL in Graz more measurements will be necessary to confirm the preliminary interpretations and assumptions, including higher statistics and the modification of the sample through the removal of the carbon layer. This modification would be of great interest since little is known about the production process of the nickel substrate and the deposition of the carbon layer. New samples will be supplied by the AVL in winter 2015/2016 and with more detailed information about their composition and production methods, interesting and promising measurements can be expected for the future.

5 Abreviations

AD – Antiproton Decelerator

ALPHA– Antihydrogen, Laser, Physics, Apparatus

AEgIS – Antimatter Experiment: Gravity Interferometry Spectroscopy

AVL - Anstalt für Verbrennungskraftmaschinen List

CERN - European Organization for Nuclear Research

e^+ - Positron

FWHM – Full Width Half Maximum

$\overline{H}$ - Antihydrogen

$\overline{H}^*$ - Excited Anithydrogen

HV – High Voltage

LINAC - Linear Accelerator

MCA - Multichannel Analyzer

MCP – Multichannel Plate

p^+ - Proton

$\overline{p}$ - Antiproton

Ps – Positronium

Ps* – Rydberg state Positronium

o-Ps – Ortho Positronium

p-Ps – Para Positronium

PMT – Photomultiplier Tube

PAS - Positron Annihilation Spectroscopy

PALS – Positron Annihilation Lifetime Spectroscopy

PS - Proton Synchrotron

RW – Rotating Wall

SSPALS – Single Shot Positron Annihilation Lifetime Spectroscopy

VEPAS - Variable Energy Positron Annihilations Spectroscopy

WEP - Weak Equivalence Principle

6 Acknowledgments

This thesis was written for the Master of Science degree at the Technical University of Graz, at the Institute for Materials Physics under the supervision of Univ.-Prof. Dr.rer.nat Roland Würschum in 2015.
Foremost, I would like to express my sincere gratitude to my advisor Prof. Roland Würschum for his guidance during the time of my master thesis, his insightful comments and suggestions for improvement.
The measurement data was obtained at the positron system of the AEgIS experiment at CERN.
I would like to thank Dr. Michael Doser for sparking my interest in antimatter physics and providing me with this great opportunity to join the AEgIS group as a technical student.
I would also like to express my sincere gratitude to Dr. Sebastiano Mariazzi, the Guru of the positron system, for his patience and support during my year in the AEgIS positron group and for all the shared knowledge.
A special thank you also to MSc. Benjamin Rienäcker and Dr. Stefan Haider, who where always open for a discussion, were fun to be around and had all the answers.
I would like to thank my fellow labmates Laura Resch, Ola Forslund and Ine Jernelv and the members of the AEgIS collaboration for the stimulating discussions, for night shifts spend working together, and for all the fun we have had during this year. Part of the measurements were conducted at the VEPAS laboratory in Como and I am very grateful to Prof. Dr. Rafael Ferragut for making these measurements possible and providing his time and expertise.
Last but not the least, I would like to thank my mum and dad, for always supporting me and believing in me throughout my studies and my life in general.

Bibliography

[1] G ai Baur, G Boero, A Brauksiepe, A Buzzo, W Eyrich, R Geyer, D Grzonka, J Hauffe, K Kilian, M LoVetere, et al. Production of antihydrogen. *Physics Letters B*, 368(3):251–258, 1996.

[2] G Yu Drobychev, U Gendotti, I Boscolo, H Walters, M Büchner, André Rubbia, MK Oberthaler, P Nédélec, S Zavatarelli, C Carraro, et al. Proposal for the aegis experiment at the cern antiproton decelerator (antimatter experiment: Gravity, interferometry, spectroscopy). Technical report, 2007.

[3] RJ Hughes. The equivalence principle. *Contemporary Physics*, 34(4):177–191, 1993.

[4] Don Colladay and V Alan Kostelecký. Cpt violation and the standard model. *Physical Review D*, 55(11):6760, 1997.

[5] Antonio Riotto and Mark Trodden. Recent progress in baryogenesis. *arXiv preprint hep-ph/9901362*, 1999.

[6] Michael Charlton and John W Humberston. *Positron physics*, volume 11. Cambridge University Press, 2001.

[7] Paul G Coleman. *Positron beams and their applications*. World Scientific, 2000.

[8] Peter J Schultz and Kelvin G Lynn. Interaction of positron beams with surfaces, thin films, and interfaces. *Reviews of Modern Physics*, 60(3):701, 1988.

[9] PG Coleman, L Albrecht, KO Jensen, and AB Walker. Positron backscattering from elemental solids. *Journal of Physics: Condensed Matter*, 4(50):10311, 1992.

[10] William H Cherry. Secondary electron emission produced from surfaces by positron bombardment. *Publication: PhD thesis, Princeton University, Source: Dissertation Abstracts International, Volume: 19-08.*, 1958.

[11] A Vehanen, KG Lynn, Peter J Schultz, and M Eldrup. Improved slow-positron yield using a single crystal tungsten moderator. *Applied Physics A*, 32(3):163–167, 1983.

[12] R Khatri, M Charlton, P Sferlazzo, KG Lynn, AP Mills Jr, and LO Roellig. Improvement of rare-gas solid moderators by using conical geometry. *Applied Physics Letters*, 57(22):2374–2376, 1990.

[13] A Po Mills Jr and EM Gullikson. Solid neon moderator for producing slow positrons. *Applied Physics Letters*, 49(17):1121–1123, 1986.

[14] J Störmer, A Goodyear, W Anwand, G Brauer, PG Coleman, and W Triftshäuser. Silicon carbide: a new positron moderator. *Journal of Physics: Condensed Matter*, 8(7):L89, 1996.

[15] Lowell S Brown and Gerald Gabrielse. Geonium theory: Physics of a single electron or ion in a penning trap. *Reviews of Modern Physics*, 58(1):233, 1986.

[16] Martin Deutsch. Evidence for the formation of positronium in gases. *Physical Review*, 82(3):455, 1951.

[17] Stephan Berko and Hugh N Pendleton. Positronium. *Annual Review of Nuclear and Particle Science*, 30(1):543–581, 1980.

[18] Mihail P Petkov, Marc H Weber, Kelvin G Lynn, and Kenneth P Rodbell. Porosity characterization by beam-based three-photon positron annihilation spectroscopy. *Applied Physics Letters*, 79(23):3884–3886, 2001.

[19] R Ferragut, A Calloni, A Dupasquier, G Consolati, F Quasso, MG Giammarchi, D Trezzi, W Egger, L Ravelli, MP Petkov, et al. Positronium formation in porous materials for antihydrogen production. In *Journal of Physics: Conference Series*, volume 225, page 012007. IOP Publishing, 2010.

[20] Alessandro Bettini. *Introduction to elementary particle physics*. Cambridge University Press, 2014.

[21] DB Cassidy and AP Mills. A fast detector for single-shot positron annihilation lifetime spectroscopy. *Nuclear Instruments and Methods in Physics Research Section A: Accelerators, Spectrometers, Detectors and Associated Equipment*, 580(3):1338–1343, 2007.

[22] Joseph Ladislas Wiza. Microchannel plate detectors. *Nuclear Instruments and Methods*, 162(1):587–601, 1979.

[23] Glenn F Knoll. *Radiation detection and measurement*. John Wiley & Sons, 2010.

[24] RW Siegel. Positron annihilation spectroscopy. *Annual Review of Materials Science*, 10(1):393–425, 1980.

[25] S. Mariazzi. *Application of Positron Spectroscopy for defect Charasterization*. PhD thesis, University of Trento, 2012.

[26] A Van Veen, H Schut, J De Vries, RA Hakvoort, and MR Ijpma. Analysis of positron profiling data by means of vepfit. In *4th International workshop on: Slow-positron beam techniques for solids and surfaces*, volume 218, pages 171–198. AIP Publishing, 1991.

[27] Courtesy of the VEPAS group.

[28] DB Cassidy, TH Hisakado, HWK Tom, and AP Mills Jr. Efficient production of rydberg positronium. *Physical review letters*, 108(4):043401, 2012.

[29] S Aghion, S Mariazzi, L Marx, et al. Laser excitation of the n= 3 level of positronium. Submitted, 2015.

[30] A Kellerbauer, M Amoretti, AS Belov, G Bonomi, I Boscolo, RS Brusa, Matthias Büchner, VM Byakov, L Cabaret, C Canali, et al. Proposed antimatter gravity measurement with an antihydrogen beam. *Nuclear Instruments and Methods in Physics Research Section B: Beam Interactions with Materials and Atoms*, 266(3):351–356, 2008.

[31] Stefano Aghion, O Ahlén, C Amsler, A Ariga, T Ariga, AS Belov, K Berggren, G Bonomi, P Bräunig, J Bremer, et al. A moiré deflectometer for antimatter. *Nature communications*, 5, 2014.

[32] S Aghion, O Ahlén, C Amsler, A Ariga, T Ariga, AS Belov, G Bonomi, P Bräunig, J Bremer, RS Brusa, et al. Prospects for measuring the gravitational free-fall of antihydrogen with emulsion detectors. *Journal of Instrumentation*, 8(08):P08013, 2013.

[33] MJ Collier, LV Jorgensen, OI Meshkov, DP van der Werf, and M Charlton. Development and testing of a positron accumulator for antihydrogen production. In *AIP Conference Proceedings*, pages 13–18. IOP INSTITUTE OF PHYSICS PUBLISHING LTD, 1999.

[34] Clifford M Surko, M Leventhal, and A Passner. Positron plasma in the laboratory. *Physical Review Letters*, 62(8):901, 1989.

[35] Jay Harrison Hartley. High-field penning-malmberg trap: confinement properties and use in positron accumulation. Technical report, Lawrence Livermore National Lab., CA (United States), 1997.

[36] DB Cassidy, SHM Deng, RG Greaves, and AP Mills Jr. Accumulator for the production of intense positron pulses. *Review of scientific instruments*, 77(7):073106, 2006.

[37] Tektronix. *Digital Phosphor Oscilloscope Data Sheet*, 2010.

[38] R. Caravita. Laser apparatus for exciting positronium in aegis positronium spectroscopy experiment. Master's thesis, University of Milan, 2012.

[39] S Mariazzi, P Bettotti, S Larcheri, L Toniutti, and RS Brusa. High positronium yield and emission into the vacuum from oxidized tunable nanochannels in silicon. *Physical Review B*, 81(23):235418, 2010.

[40] FJ Himpsel, JA Knapp, JA VanVechten, and DE Eastman. Quantum photoyield of diamond (111) stable negative-affinity emitter. *Physical Review B*, 20(2):624, 1979.

[41] RH Howell, IJ Rosenberg, MJ Fluss, RE Goldberg, and RB Laughlin. Positronium time-of-flight spectroscopy of dissimilar metals. *Physical Review B*, 35(10):5303, 1987.

[42] S Aghion, S Mariazzi, L Marx, et al. Positron bunching and electrostatic transport system for the production and emission of dense positronium clouds into vacuum. *Nuclear Instruments and Methods in Physics Research Section B: Beam Interactions with Materials and Atoms*, 362:86–92, 2015.

[43] Søren L Andersen, Rasmus R Johansen, Jakob B Overgaard, Johan K Mortensen, Kristoffer K Andersen, Heine D Thomsen, Mikkel D Lund, Jacques Chevallier, Helge Knudsen, and Ulrik I Uggerhøj. Positronium formation from porous silica in backscattering and transmission geometries. *The European Physical Journal D*, 68(5):1–6, 2014.

[44] Allen P Mills Jr. Positronium formation at surfaces. *Physical Review Letters*, 41(26):1828, 1978.